DOT HS 806 961
DOT TSC NHTSA-85 5

Crash Padding R s arch
Volume II: Constitutive Equation Models

Oscar Orringer
Kevin T Knadle
John F Mandell

Transportation Systems Center
Cambridge MA 02142

August 1986
Final Report

US Department of Transportation
National Highway Traffic Safety Administration

Office of Research and Development
Office of Crashworthiness Research
Washington DC 20590

Technical Report Documentation Page

1. Report No.	2 Government Accession No.	3 Recipient's Catalog No.
DOT-HS-806-961		

4. Title and Subtitle	5 Report Date
CRASH PADDING RESEARCH Volume II: Constitutive Equation Models	August 1986
	6 Performing Organization Code DTS-44
7 Author(s) Oscar Orringer, Kevin T. Knadle,* John F. Mandell*	8. Performing Organization Report No. DOT-TSC-NHTSA-85-5
9. Performing Organization Name and Address U.S. Department of Transportation Research and Special Programs Administration Transportation Systems Center Cambridge, MA 02142	10 Work Unit No (TRAIS) HS676/S6508
	11 Contract or Grant No.
12. Sponsoring Agency Name and Address U.S. Department of Transportation National Highway Traffic Safety Administration Office of Research and Development Washington, DC 20590	13. Type of Report and Period Covered Final Report April 1982 - June 1984
	14. Sponsoring Agency Code NRD-10

15. Supplementary Notes

*Department of Materials Science and Engineering
Massachusetts Institute of Technology
Cambridge, MA 02139

16. Abstract

Several simplified one-dimensional constitutive equations for viscoelastic materials are reviewed and found to be inadequate for representing the impact-response performance of strongly nonlinear materials. Two multi-parameter empirical models are developed in accordance with consistency criteria which assure the existence of a constitutive equation. Curve-fitting procedures are derived for each model, and the models are applied to test data previously developed for Uniroyal Ensolite AAC foam rubber. The accuracy of dynamic performance representation provided by each model is assessed.

17. Key Words	18. Distribution Statement
Crash Padding, Mechanical Properties, Viscoelastic Materials, Constitutive Equation, State Equation	Document is available to the public through the National Technical Information Service, Springfield, VA 22161

19 Security Classif. (of this report)	20. Security Classif. (of this page)	21. No. of Pages	22. Price
UNCLASSIFIED	UNCLASSIFIED	64	

Form DOT F 1700.7 (8-72) Reproduction of completed page authorized

PREFACE

The analytical work described herein was conducted at the DOT Transportation Systems Center, Cambridge, Massachusetts. The experimental work was conducted at the Massachusetts Institute of Technology, Cambridge, Massachusetts. The work was sponsored by the National Highway Traffic Safety Administration under Project Plan Agreement HS-476. This series of reports is specifically concerned with evaluating the impact response characteristics of foam-type crash padding materials. This report is the second of three volumes in the series. Volume I covered the results of laboratory tests to determine the basic dynamic mechanical properties of a typical foam rubber. This report covers the derivation of foam-rubber constitutive equation models and the procedures used to fit the model parameters to the laboratory test results. Volume III will cover application and validation of the best model for impact response prediction.

METRIC CONVERSION FACTORS

Approximate Conversions to Metric Measures

Symbol	When You Know	Multiply by	To Find	Symbol
		LENGTH		
in	inches	*2 5	centimeters	cm
ft	feet	30	centimeters	cm
yd	yards	0 9	meters	m
mi	miles	1 6	kilometers	km
		AREA		
in^2	square inches	6 5	square centimeters	cm^2
ft^2	square feet	0 09	square meters	m^2
yd^2	square yards	0.8	square meters	m^2
mi^2	square miles	2 6	square kilometers	km^2
	acres	0 4	hectares	ha
		MASS (weight)		
oz	ounces	28	grams	g
lb	pounds	0 45	kilograms	kg
	short tons (2000 lb)	0.9	tonnes	t
		VOLUME		
tsp	teaspoons	5	milliliters	ml
Tbsp	tablespoons	15	milliliters	ml
fl oz	fluid ounces	30	milliliters	ml
c	cups	0 24	liters	l
pt	pints	0 47	liters	l
qt	quarts	0 95	liters	l
gal	gallons	3 8	liters	l
ft^3	cubic feet	0 03	cubic meters	m^3
yd^3	cubic yards	0 76	cubic meters	m^3
		TEMPERATURE (exact)		
°F	Fahrenheit temperature	b/9 (after subtracting 32)	Celsius temperature	°C

*1 in. = 2 54 cm (exactly) For other exact conversions and more detail tables see NBS Misc. Publ 286 Units of Weight and Measures. Price $2.25 SD Catalog No. C13 10 286

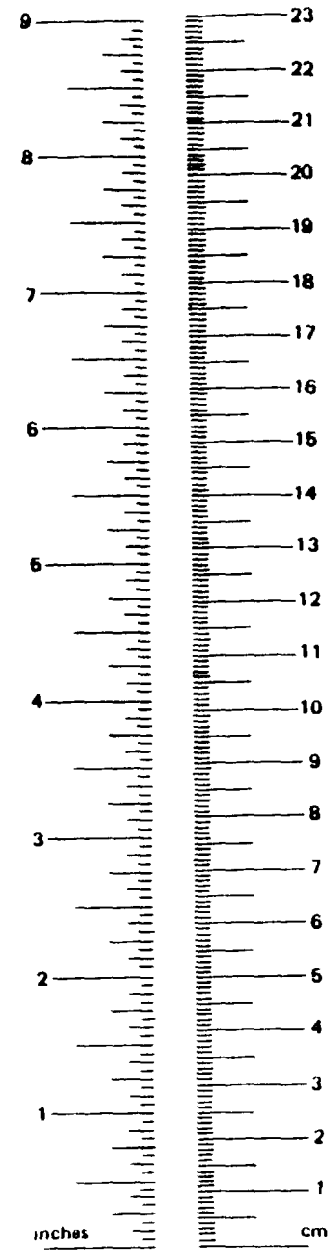

Approximate Conversions from Metric Measures

Symbol	When You Know	Multiply by	To Find	Symbol
		LENGTH		
mm	millimeters	0 04	inches	in
cm	centimeters	0 4	inches	in
m	meters	3 3	feet	ft
m	meters	1 1	yards	yd
km	kilometers	0 6	miles	mi
		AREA		
cm^2	square centimeters	0 16	square inches	in^2
m^2	square meters	1 2	square yards	yd^2
km^2	square kilometers	0 4	square miles	mi^2
ha	hectares (10,000 m^2)	2 5	acres	
		MASS (weight)		
g	grams	0 035	ounces	oz
kg	kilograms	2 2	pounds	lb
t	tonnes (1000 kg)	1 1	short tons	
		VOLUME		
ml	milliliters	0 03	fluid ounces	fl oz
l	liters	2 1	pints	pt
l	liters	1 06	quarts	qt
l	liters	0 26	gallons	gal
m^3	cubic meters	36	cubic feet	ft^3
m^3	cubic meters	1 3	cubic yards	yd^3
		TEMPERATURE (exact)		
°C	Celsius temperature	9/5 (then add 32)	Fahrenheit temperature	°F

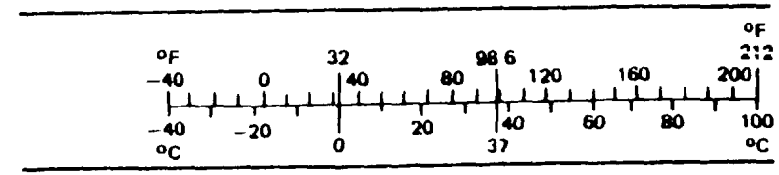

TABLE OF CONTENTS

LIST OF ILLUSTRATIONS

LIST OF TABLES

SUMMARY

Selection of materials for energy-absorbent performance is an important consideration for automobile interior padding, which must provide the greatest occupant protection for the least padding thickness possible. Rational selection requires an understanding of which material properties, as measured in standard laboratory tests, correlate well with impact performance in crash situations. Such understanding can be gained by characterizing a material in the laboratory, constructing a performance model from the laboratory test results, applying the model to predict the response of the material to impact conditions, and then verifying the prediction by test.

Volume I of this series of reports summarized the first link in the chain of understanding: results of laboratory tests to determine the dynamic properties of Uniroyal Ensolite AAC foam rubber, a typical crash padding product which the National Highway Traffic Safety Administration has used in other investigations of injury mitigation concepts for automobile occupants.

This report is Volume II of the series, and summarizes the results of the second link. Earlier methods for constructing material performance models were reviewed and were found to be inadequate for representing the impact response characteristics of materials like Ensolite foam rubber. Criteria were then formulated for the more complex type of model required, and two such models were developed. The model developments included organization of curve-fitting procedures which take advantage of all of the relevant materials test data.

When the two models were applied to the Ensolite test data, one was found to accurately represent the material over only a limited range of performance, but the second was found to represent the material well over the entire range of interest. Both models may still be useful for predicting the impact response of Ensolite AAC, and both models can be applied to other materials.

1. INTRODUCTION

The first volume of this report summarized the results of laboratory tests to determine the compressive mechanical properties of Uniroyal Ensolite AAC foam rubber, a recoverable closed-cell crash padding material. The principal results were for stress as a function of time after imposition of a fixed strain (stress relaxation) and for stress as a function of strain applied at a fixed rate. The second group of results included measurements of the "residual" strain present at the instant the material had unloaded to zero stress. Both groups of results were extrapolated to typical impact times (0.001 second) and strain rates (2,000 per second) by means of the time-temperature superposition principle, which was used to construct master curves for material behavior at 25°C from results of tests at lower temperatures.

The body of data in Volume I characterizes the material response to two specific types of loading. This characterization of material properties must be generalized, however, to provide a useful basis for predicting the dynamic responses of objects which collide with padded structure. What is sought is an equation of state, or constitutive equation, which describes the possible relationships between current states and incremental changes of stress and strain in the material.

In the typical impact situation, the colliding mass imposes a known initial strain rate on the crash padding material. The mass is decelerated and the strain rate decreases, however, as the padding builds up stress to resist the motion of the mass. The deceleration eventually brings the mass to momentary rest with respect to the padding, the relative motion is then reversed, and finally there occurs an instant when the padding stress has returned to zero. At this last instant, contact between the mass and padding is lost, and the impact event is complete.

To be useful for predicting impact response, a constitutive equation must be able to follow all of the foregoing phases of the motion. This imposes the following three requirements on the properties of the equation itself. First, as a minimum, it must relate the instantaneous rate of change of stress to the instantaneous values of stress, strain, and strain rate. Second, it must embody an unambiguous relationship between loading and unloading, including transitions between these states at zero strain rate. Third, it must account for the presence of residual strain rate in the padding at the end of contact.

In addition to satisfying the foregoing requirements, the constitutive equation must also be consistent with the laboratory test data and should have as simple a form as possible. This volume summarizes the development of such constitutive equation models for the one-dimensional (uniform compression) behavior of Ensolite foam rubber. Section 2 reviews several earlier models which were investigated, but which were found to have various significant limitations. As a consequence of these initial studies, some general mathematical criteria were formulated to govern the construction of multi-parameter empirical models, and two such models were derived. Section 3 discusses these developments, including the analysis procedures used to fit the models to laboratory test data. Section 4 describes the numerical results obtained by applying the curve-fitting procedures to the Volume I test data for Ensolite foam and illustrates the degree of consistency obtained.

2. REVIEW OF EARLIER MODELS

Three previously published models were investigated for possible application of the prediction of Ensolite foam rubber impact response. The first of these was the classical linear viscoelastic solid (LVS), and the investigation also included some extensions of the LVS to nonlinear behavior. The second and third were empirical models based on experiments peformed by other investigators. None of these models had enough parametric flexibility to describe the behavior of Ensolite foam rubber.

2.1 THE LINEAR VISCOELASTIC SOLID

The constitutive equation of the linear viscoelastic solid is given by [1]:

$$\dot{\sigma} + \sigma/\tau + E_0\dot{\varepsilon} + E_\infty\varepsilon/\tau \tag{1}$$

where σ and ε are the material stress and strain, respectively, and where a dot over a quantity indicates a time derivative.

The parameters of the LVS model have the following meanings. The parameter E_0 is an "instantaneous" elastic modulus, i.e., it expresses the stress-strain relation for the idealized limit of infinite strain rate. The parameter E_∞ is a fully relaxed elastic modulus, i.e. it expresses the stress-strain relation for the idealized limit of zero strain rate. The linearity of the LVS model refers to these asymptotic stress-strain relations. The parameter τ is a characteristic decay time, i.e. the amount of time (after a suddenly imposed strain) that is required for the stress to decrease to the fraction 1/e of its instantaneous value.

The LVS is often interpreted in terms of the spring-and-damper analog shown in Figure 2-1. The spring represented by E_0 models the elastic "instantaneous" stage, while the time-dependent stage is represented by the parallel combination of spring E_1 and damper C_1. The stress σ is proportional to a strain ε_0 across the first stage, but $\sigma=E_1\varepsilon_1+C_1\dot{\varepsilon}_1$ across the second stage. The constitutive relation of Eq. 1 is obtained by expressing the model in terms of total strain ε, and defining:

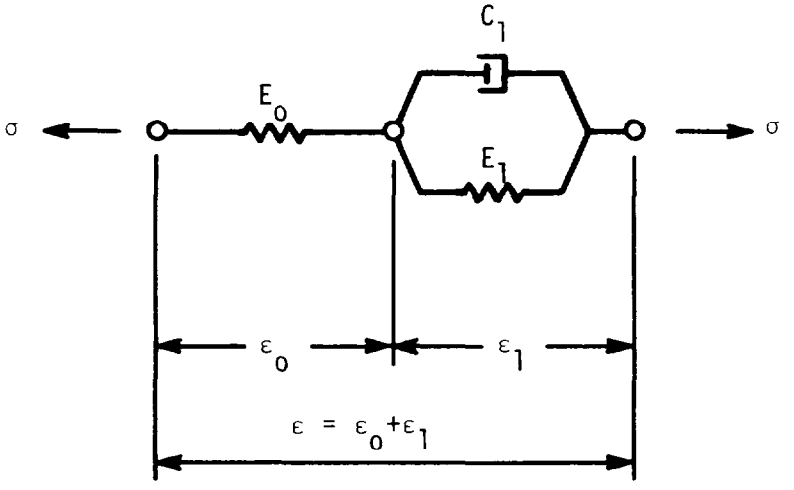

FIGURE 2-1. SPRING-AND-DAMPER ANALOG OF LVS MODEL

$$E_\infty = E_0E_1/(E_0+E_1) \quad \tau = C_1/(E_0+E_1) \tag{2}$$

If the strain and strain rate are prescribed in any self-consistent manner, the LVS constitutive equation has the following general solution for the stress-time history:

$$\sigma(t) = e^{-t/\tau}\left[A + \int (E_0\dot{\varepsilon}+E_\infty\varepsilon/\tau)e^{t/\tau}dt\right] \tag{3}$$

where A is a constant whose value is determined by the initial conditions at t = 0. The general solution of Eq. 3 includes the so-called hereditary integral solution, which is usually expressed in the definite-integral form:

$$\sigma(t) = E(t)\varepsilon(o) + \int_0^t E(t-t')\dot{\varepsilon}(t')dt' \tag{4}$$

where

$$E(t) = E_\infty + (E_o - E_\infty)e^{-t/\tau} \tag{5}$$

is the so-called relaxation modulus. The following stress solutions for specific applied strain-time histories are of interest.

2.1.1 Idealized Stress-Relaxation Test

A strain ε is suddenly applied at t = 0 and is held constant for t > 0. The stress response for $t \geq 0$ is:

$$\sigma(t) = E(t)\varepsilon \tag{6}$$

Note that the stress-relaxation behavior of the material is characterized by a unique master curve: the relaxation modulus.

2.1.2 Loading at Constant Strain Rate

Strain is applied at a constant rate $\dot{\varepsilon}$, beginning at t = 0. Thus, $\varepsilon(t) = \dot{\varepsilon}\, t$ and the stress response for $t \geq 0$ is given by:

$$\sigma(t) = \left[E_\infty + (E_0 - E_\infty) \left(\frac{1 - e^{-t/\tau}}{t/\tau} \right) \right] \dot{\varepsilon} t \tag{7}$$

Equation 7 embodies the linear asymptotic properties for the limits of zero and infinite strain rate. For finite strain rates, the stress-strain curve has a slight nonlinearity but the amount and its characteristics are not flexible enough to allow curve-fitting to strongly nonlinear materials.

2.1.3 Idealized Stress-Strain Test

Beginning at t = 0, strain is applied at a constant rate $\dot{\varepsilon}$ for a finite time ($\varepsilon/\dot{\varepsilon}$) until a maximum strain ε is achieved. At $t = \varepsilon/\dot{\varepsilon}$, the rate of strain application is instantaneously reversed, and the material is allowed to unload. The stress response for $0 \leq t \leq \varepsilon/\dot{\varepsilon}$ is given by Eq. 7, and at the instant of reversal:

$$\sigma(\varepsilon/\dot{\varepsilon}) = E_\infty \varepsilon + (E_0 - E_\infty)(1 - e^{-\varepsilon/\dot{\varepsilon}\tau})\, \dot{\varepsilon}\tau \tag{8}$$

For $t \geq \varepsilon/\dot{\varepsilon}$, ie. the unloading phase, the stress response is given by:

$$\begin{aligned} \sigma(t) = {} & 2(E_\infty \varepsilon + E_0 \dot{\varepsilon}\tau) e^{\varepsilon/\dot{\varepsilon}\tau}\, e^{-t/\tau} - (E_0 - E_\infty)\dot{\varepsilon}\tau e^{-t/\tau} \\ & + E_\infty(\dot{\varepsilon}t - \dot{\varepsilon}\tau - 2\varepsilon) - E_0 \dot{\varepsilon}\tau \end{aligned} \tag{9}$$

A plot of the loading-unloading response would reveal a slight hysteresis effect and a small residual strain at the point where $\sigma(t)$, as calculated by Eq. 9, returns to zero. Like 2.1.2, however, these characteristics are not flexible enough to allow curve-fitting to strongly nonlinear materials.

2.1.4 Steady-State Sinusoidal Response

A strain $\varepsilon(t) = \varepsilon \sin\omega t$ is applied to the material with a constant strain amplitude ε and a fixed frequency ω. The strain rate is also sinusoidal, $\dot{\varepsilon}(t) = \omega\varepsilon \cos \omega t$

The stress response (after sufficient time to damp out transients has elapsed) is a sinusoid that lags the strain input by a phase angle ϕ :

$$\sigma(t) = \sigma\sin(\omega t + \phi) \tag{10}$$

where

$$\tan\phi = \frac{(E_o/E_\infty - 1)\omega\tau}{1 + (E_o/E_\infty)\ (\omega\tau)^2} \tag{11}$$

$$\sigma = E_\infty\varepsilon\sqrt{\frac{1 + (E_o\omega\tau/E_\infty)^2}{1 + (\omega\tau)^2}} \tag{12}$$

The solution is sometimes expressed in terms of the equivalent complex moduli E' and E" as follows:

$$\sigma(t) = (E' + iE'')\varepsilon \sin(\omega t) \tag{13}$$

where

$$E' = \frac{E_\infty + E_o(\omega\tau)^2}{1 + (\omega\tau)^2} \tag{14}$$

$$E'' = \frac{(E_o - E_\infty)\omega\tau}{1 + (\omega\tau)^2} \tag{15}$$

and where

$$\tan\phi = E''/E' \quad \sigma = \varepsilon\sqrt{(E')^2 + (E'')^2} \tag{16}$$

Steady-state sinusoidal response tests are often used to characterize the vibratory damping properties of viscoelastic materials. The damping factor can be related to the energy loss per cycle of sinusoidal motion, and the energy loss is proportional to tan ϕ . The LVS model has a loss-tangent characteristic with a unique maximum at the frequency:

$$\omega = \frac{1}{\tau}\sqrt{E_\infty/E_o} \tag{17}$$

However, real viscoelastic materials tend to have loss tangents which are flat over a wide frequency range, or which possess several weak local maxima.

2.2 COMMENT ON LVS MODEL

Before the other models are discussed, it is worthwhile to recognize the influence that the LVS model has exerted on viscoelastic materials research. The LVS model is attractive for three reasons. The first is its convenient physical interpretation (Figure 2-1).

The second reason is the ease with which analytical solutions to dynamic problems can be obtained from the LVS model. Several examples simulating laboratory tests were mentioned in Section 2.1, but even some impact situations can be similarly analyzed. For example, consider the problem of a rigid mass M which strikes a rigidly supported LVS pad of cross section area A and thickness L; the mass is further assumed to have a flat face and the same cross section as the pad, so that the material will be subjected to uniform compression (Figure 2-2). The mass has an initial velocity V and is decelerated after contact ($t > 0$) in accordance with:

$$M\ddot{x} = -\sigma A \tag{18}$$

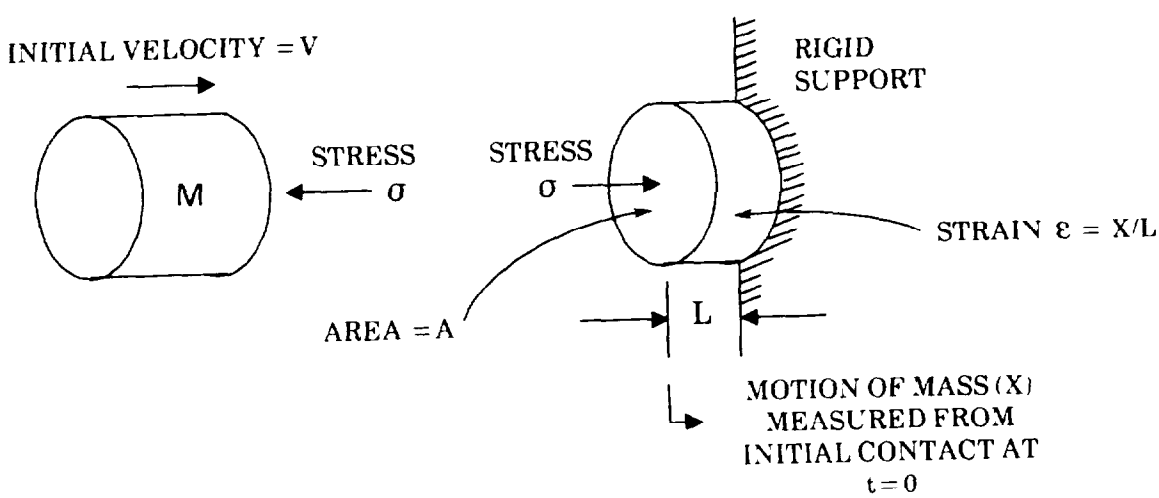

FIGURE 2-2. A FREE-IMPACT PROBLEM

Under the foregoing assumptions, it is easy to show that Eq. 18 can be combined with the LVS constitutive equation (Eq. 1) to obtain:

$$\dddot{\sigma} + \ddot{\sigma}/\tau + E_o A\dot{\sigma}/ML + E_\infty A\sigma/ML\tau = 0 \tag{19}$$

subject to the initial conditions

$$\sigma=o;\ \dot{\sigma} = E_o V/L;\quad \ddot{\sigma} = (E_\infty - E_o)V/L\tau \tag{20}$$

at t = 0. The solution can then be expressed immediately in the form:

$$\sigma(t) = A_1 e^{\lambda_1 t} + A_2 e^{\lambda_2 t} + A_3 e^{\lambda_3 t} \tag{21}$$

where λ_1, λ_2, λ_3 are the roots of the characteristic polynomial corresponding to Eq. 19 and A_1, A_2, A_3 are determined from Eq. 20.

The third reason is that the LVS model displays all its parameters directly for any type of laboratory test. Thus, only a few data points from one type of test are required to fit the parameters, if one accepts a priori that the LVS is a reasonable model of the test material. If the stresses $\sigma_1 = \sigma(t_1)$, $\sigma_2 = \sigma(t_2)$. and the stress asymptote σ_∞ are obtained from a stress-relaxation test at one strain ε, for example, the LVS model parameters are given by:

$$E_\infty = \sigma_\infty/\varepsilon \tag{22}$$

$$E_o = E_\infty + (\sigma_1 - \sigma_\infty)^{m+1}/(\sigma_2 - \sigma_\infty)^m \tag{23}$$

$$\tau = (t_2 - t_1)\ \log_e\left[(\sigma_1 - \sigma_\infty)/(\sigma_2 - \sigma_\infty)\right]$$
$$m = t_1/(t_2 - t_1). \tag{24}$$

where $m = t_1/(t_2-t_1)$.

The LVS is a useful conceptual model because it combines the major characteristics of viscoelastic behavior with convenience in curve-fitting and dynamic analysis. As attractive as this combination is, however, one should avoid the temptation to force-fit real material test data into the LVS mold.

2.3 EXTENSION OF SPRING-DAMPER ANALOG MODELS

Spring-damper analogs such as the one shown in Figure 2-1 have served as points of departure for modelling complex aspects of viscoelastic behavior. One of the traditional approaches is to add more linear components to the model, each component representing one more parametric degree of freedom. This approach has been extensively used, for example, to construct models of relaxation for real polymers which possess multiple relaxation mechanisms with distinct characteristic decay times [3].

A different approach was taken in the present investigation in order to model different types of stress-strain curve nonlinearity. Single-component modifications or additions were made to the baseline configuration of Figure 2-1 to individually model two specific stress-strain nonlinearities.

In the first model, a softening characteristic was obtained by modifying the elastic spring E_o as shown in Figure 2-3. The constitutive equation for this model is:

$$\left[1 + n(E_o/B)(\sigma/B)^{n-1}\right]\dot{\sigma} = E_\infty \varepsilon/\tau + E_o\dot{\varepsilon} - \left[1 + (E_\infty/B)(\sigma/B)^{n-1}\right]\sigma/\tau \tag{25}$$

where the material parameters E_o, E_∞ , B are moduli, τ is the characteristic time and $n > 1$ is a dimensionless, exponent. At the limit of zero strain rate, the behavior of this model follows the Ramberg-Osgood stress-strain relation:

$$\varepsilon = \sigma/E_\infty + (\sigma/B)^n \tag{26}$$

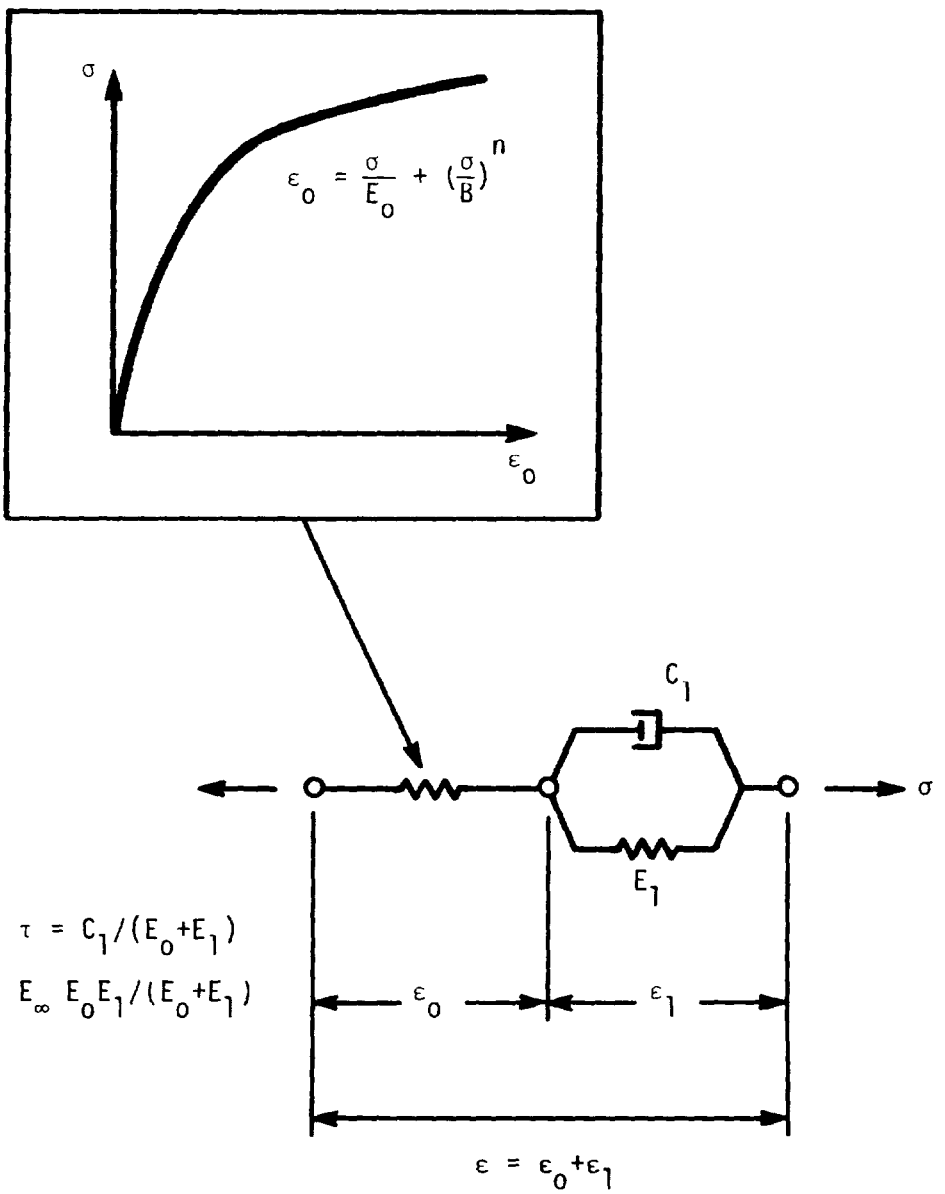

FIGURE 2-3. SPRING-DAMPER MODEL WITH SOFTENING CHARACTERISTIC

Figure 2-4 illustrates the second model, which produces the stiffening behavior with a constitutive equation of the form:

$$\dot{\sigma} = (E_\infty + B\varepsilon^{n-1})\dot{\varepsilon}/\tau + (E_0 + nB\varepsilon^{n-1})\cdot - \sigma/\tau \tag{27}$$

The material parameters play the same roles as in the softening model, but B and n have different interpretations. The asymptotic behavior in this case is:

$$\sigma = E_\infty \varepsilon + B\varepsilon^n \tag{28}$$

The equations of both models are restricted to the compression side of the stress-strain diagram, but the strain rate and stress rate can be either positive or negative. Both models possess the undesirable feature that they permit strains $\varepsilon > 1$ unless limited by auxiliary logic.

Numerical simulations were run to investigate the behavior of the non-linear-spring models. The next three figures illustrate some typical results obtained from a softening model. Figure 2-5 plots a family of stress-relaxation curves for several different strains. The curve tends to flatten at larger values of applied strain. Figure 2-6 compares the static stress-strain curve with a simulation of stress-strain tests at a constant strain rate. The simulation includes the unloading as well as the loading phase to demonstrate the hysteresis embodied in the model. The strain rate used in the simulation was chosen to maximize the width of the hysteresis loop. Figure 2-7 compares this case with simulations at higher and lower strain rates. Similar behavior characteristics were found for the stiffening model. The HP67 programs used to run these simulations appear in Appendix A.

The change in the shape of the stress-relaxation curve as a function of applied strain and the softening or stiffening characteristics of stress-strain curves are all features found in the behavior of real viscoelastic materials. However, the nonlinear-spring models were found to have only limited abilities to reproduce these features. For example, the tendency of the hysteresis effect to peak at a finite strain rate in the model (Figure 2-7) is fundamentally different from the tendency of a steady increase of hysteresis with increasing strain rate in Ensolite foam rubber (Figure 2-8). Therefore, the nonlinear-spring models were judged to be unsuitable to represent real material behavior.

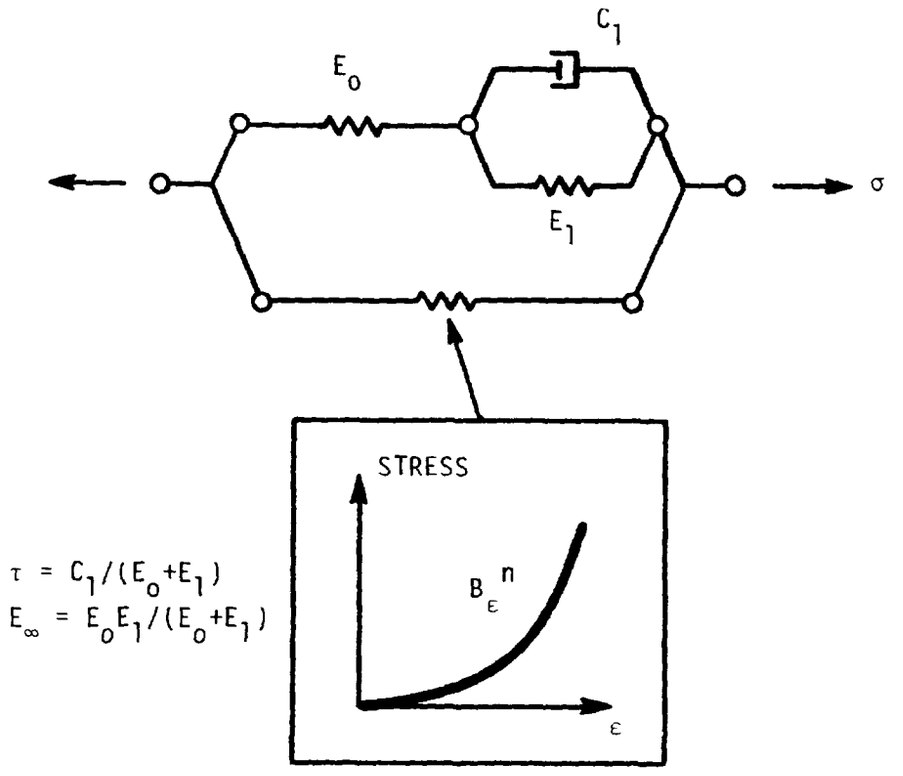

FIGURE 2-4. SPRING-DAMPER MODEL WITH STIFFENING CHARACTERISTIC

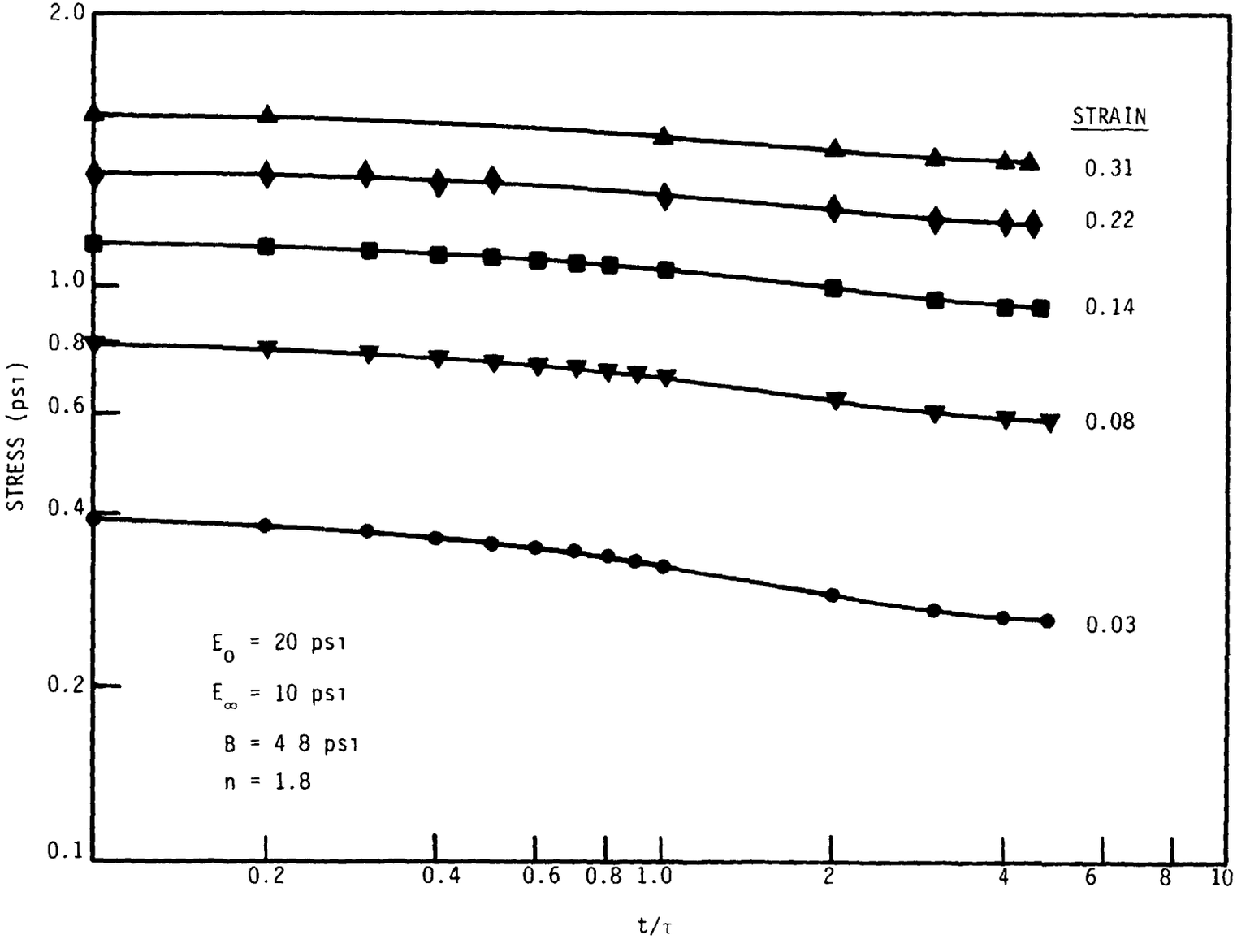

FIGURE 2-5. STRESS-RELAXATION RESPONSE OF SOFTENING MODEL

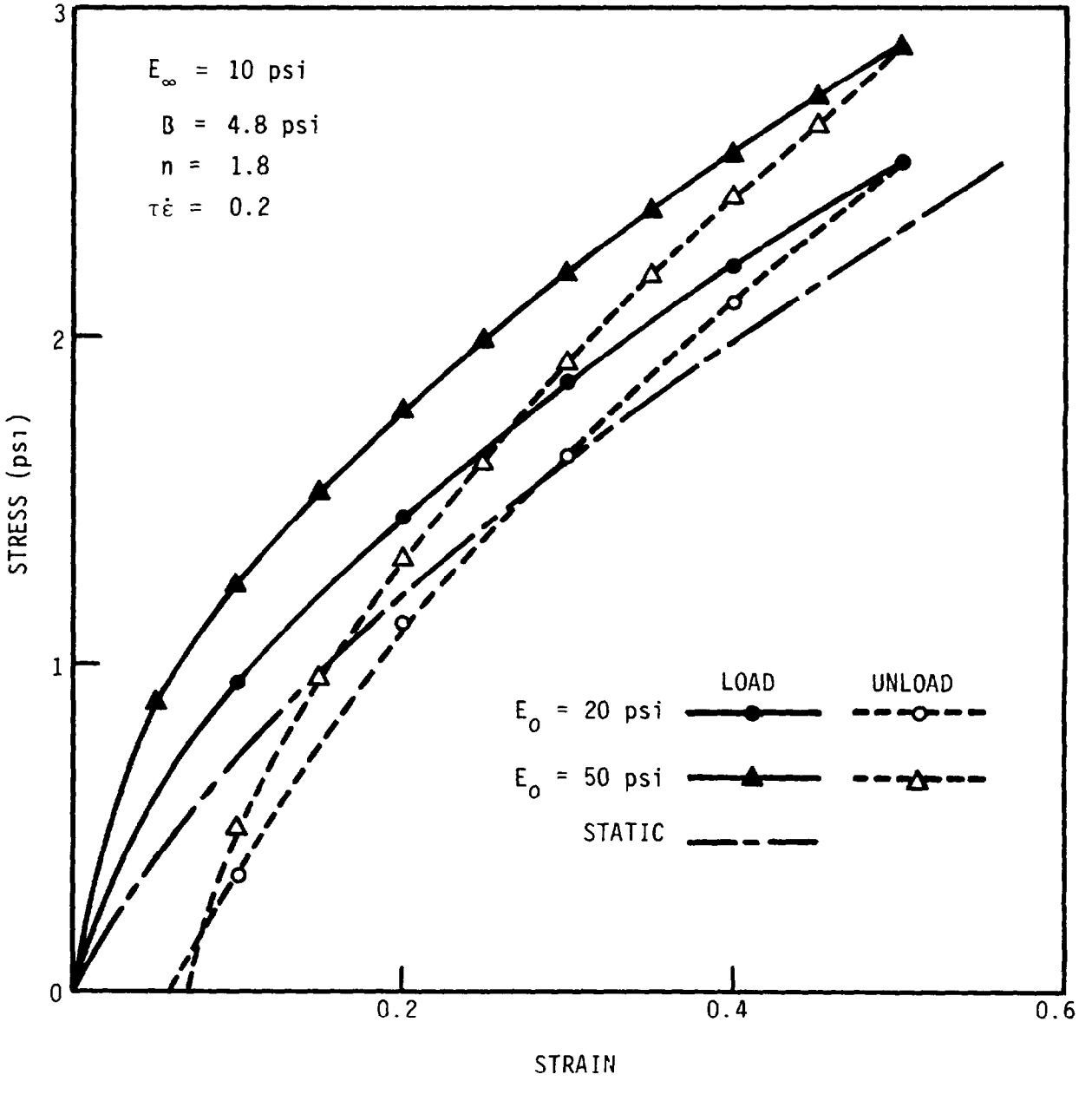

FIGURE 2-6. STATIC AND DYNAMIC STRESS-STRAIN CURVES FOR SOFTENING MODEL

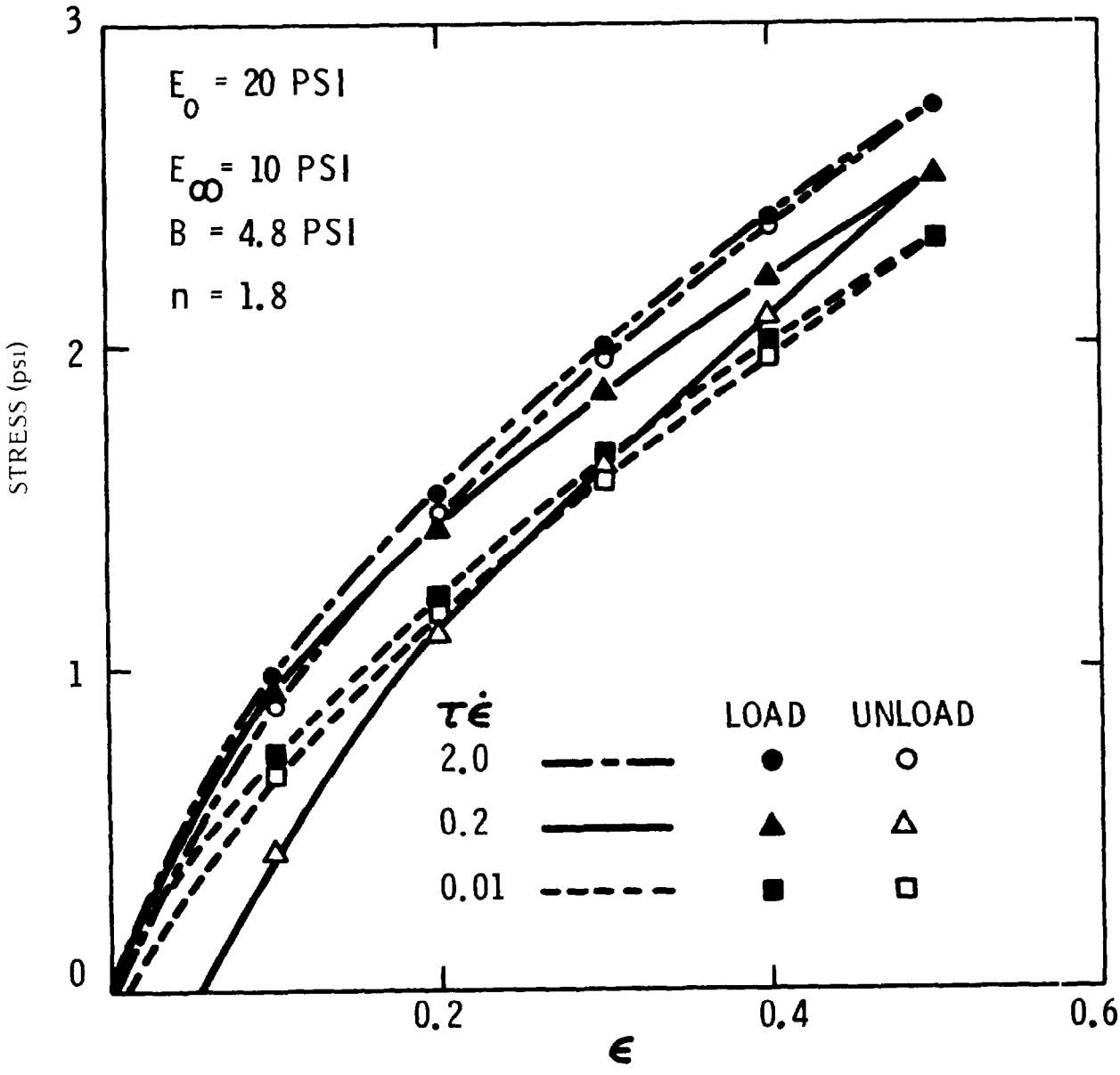

FIGURE 2-7. ILLUSTRATION OF LIMITED ABILITY TO MODEL HYSTERESIS EFFECT

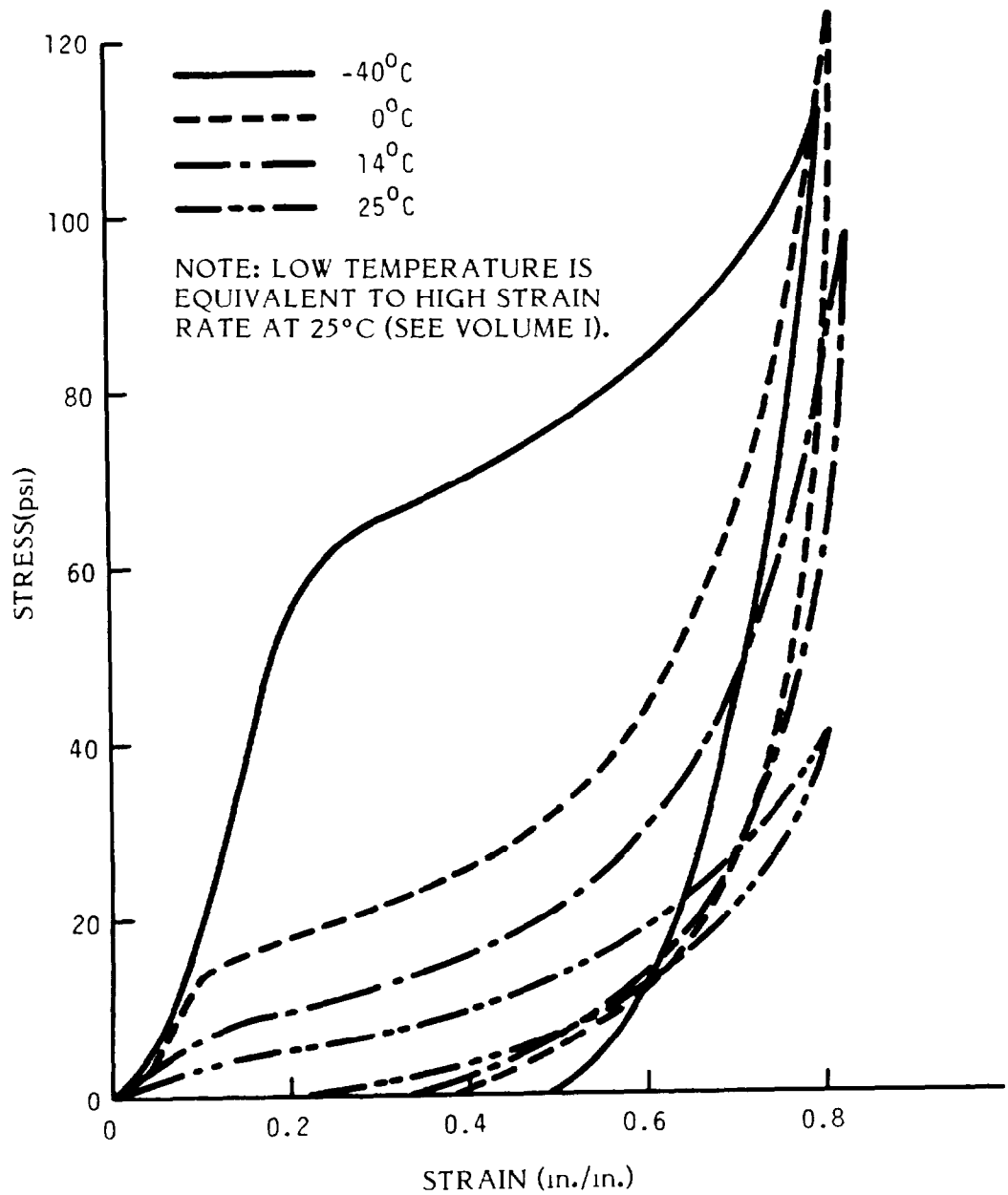

FIGURE 2-8. ENSOLITE AAC FOAM RUBBER STRESS-STRAIN CURVES AT LOW STRAIN RATE

2.4 EMPIRICAL MODELS

Two empirical models proposed by other investigators were examined. Both models are based on an approach of direct curve fitting to a single kind of laboratory test data.

2.4.1 Power-Law Model for Stress Relaxation

Meinecke and Clark [4] have proposed a power-law representation in the time domain to fit stress-relaxation data. The model also includes an asymptotic stress-strain nonlinearity. The empirical equation for this model is:

$$\sigma(t;\varepsilon) = \varepsilon E(\varepsilon) t^{-n} \tag{29}$$

where ε is the fixed strain applied in the stress-relaxation test and $E(\varepsilon)$ embodies the stress-strain nonlinearity. Since Eq. 29 implies arbitrarily high stresses at arbitrarily short times, however, it is better to express the power-law model in the form:

$$\sigma(t;\varepsilon) = \varepsilon E(\varepsilon) \left(\frac{t+t_o}{t_o} \right)^{-n} \tag{30}$$

where it is defined that $\varepsilon E(\varepsilon)$ is the first stress observation at time t_o after the experiment has started, and where the model is implicitly restricted to times after the first observation.

The time scale, t, in Eq. 30 has been shifted such that $t = 0$ corresponds to the first observation point. Under these arrangements a hereditary integral can be used to extend the power-law model to situations other than the stress-relaxation test. For example, the response of stress to strain applied at a constant rate $\dot{\varepsilon}$ would be predicted by:

$$\sigma(t,\dot{\varepsilon}) = t_o \dot{\varepsilon}\, E(t\dot{\varepsilon}) + \dot{\varepsilon} \int_0^t E\left[(t-t')\dot{\varepsilon}\right] \left(\frac{t+t_o-t'}{t_o} \right)^{-n} dt' \tag{31}$$

where $E(t\dot{\varepsilon})$ is the value of $E(\varepsilon)$ at time t.

The model of Eq. 29 has been used to fit the stress-relaxation behavior of several foam-rubber materials [4] and equivalent fits could easily be made with Eq. 30. However, the data available for fitting spanned 0.1 to 10^4 seconds after test start, i.e. times much longer than the expected durations of typical impacts. Even if shorter-time data were available, fitting the stress-relaxation data would still not guarantee that Eq. 31 could correctly predict the hysteresis effects associated with impact response. Also, the power-law model does not lend itself well to the formulation of a true constitutive equation, and is thus computationally inconvenient.

2.4.2 Power-Law Strain-Rate Model

Recent work in the United Kingdom (UK) included investigation of six rigid and nine semi-rigid foams[5] . In this study, the investigators obtained stress-strain curves at several different constant strain rates and used the data to fit models of the form:

$$\sigma(\varepsilon,\dot{\varepsilon}) = f(\varepsilon)\dot{\varepsilon}^{r} \tag{32}$$

For strains up to 0.5 in the rigid foams they found that $f(\varepsilon)$ is close to a constant for each material, while the strain-rate exponent, r, ranged from 0.02 to 0.08 for the six materials. The small exponent values suggest that such materials can be adequately represented by two parameters: a crush strength and a limit strain. Beyond the limit strain, the foam cell structure must be considered to have completely collapsed, and the pad stiffness would then be controlled by the mechanical properties of the solid material from which the foam is made. For the semi-rigid foams the investigators were able to fit the material test data reasonably well with the empirical equation:

$$\sigma(\varepsilon,\dot{\varepsilon}) = E\dot{\varepsilon}^{r}/(1-\varepsilon)^{n} \tag{33}$$

where E,n, and r are the parameters. The strain-rate exponent, r, ranged from 0.04 to 0.3 for the nine semi-rigid foams studied.

The UK work was also correlated with impact-simulation tests in which rigid spheres were allowed to strike rigidly supported pads at speeds of about 6 mph. A load cell in series with the supporting structure measured the time-history of the total force F acting on the pad. Force-time history predictions were made by taking:

$$F = \sigma(\varepsilon,\dot{\varepsilon})A \tag{34}$$

where A is the contact area on the pad (linearized in terms of the sphere penetration Xp, assumed to be much smaller than the sphere's radius), and where three-dimensional effects of the nonuniform contact were neglected. The agreement between predicted and measured force during the penetration phase of the impact was excellent for the rigid materials, which were also observed to have Poisson's ratios close to zero. The predictions for semi-rigid foams were somewhat in error, a result which was attributed to three-dimensional effects.

The foregoing model appears to be most useful for rigid foams and within the confines of those situations that have been studied experimentally. The model is not well suited to predicting the unloading and rebound characteristics of semi-rigid foam pads, however, and is impossible to reconcile with data from stress-relaxation tests because Eq. 32 implies that $\sigma(t) = 0$ for all times after the applied strain is held constant.

3. DEVELOPMENT OF MULTI-PARAMETER EMPIRICAL MODELS

The viscoelastic material models discussed in Section 2 have a common feature: each employs a few parameters to match one aspect of material behavior. Even if the model can reproduce the matched aspect accurately, however, it is questionable if other important aspects can be reproduced.

Nonlinear-spring models can match nonlinear asymptotic stress-strain curves but are unable to reproduce realistic hysteresis effects or stress-relaxation behavior. The power-law model for stress relaxation can be fitted to relaxation data but not to hysteresis effects, and it is not per se a constitutive equation. The power-law strain-rate model can match nonlinear stress-strain curves and (to some extent) the effect of finite strain rates on the loading phase but is inconsistent with stress relaxation and asymptotic behavior at zero strain rate.

Consequently, the present investigators decided to try an empirical approach without restriction on the number of model parameters but with emphasis on matching as many aspects of uniform compression behavior as could be gleaned from the laboratory test data reported in Volume I. The approach was constrained by some general conditions of consistency, which candidate models were required to satisfy. Two such empirical models were formulated: one with 9 and one with 21 parameters. The development also encompassed an organized procedure for fitting the models to the test data.

3.1 CONDITIONS OF CONSISTENCY

Four behavior characteristics of viscoelastic materials are significant for the impact situation and should be modelled independently to avoid the limitations of the earlier models. These characteristics are as follows.

First, the stress-relaxation curve must influence the response of stress to changing strain rate. Although the stress-relaxation curve itself corresponds to a state of fixed strain and zero strain rate, the material behavior exhibited in this test reflects an "inertial" property that forbids discontinuous changes in stress, even when the strain rate changes discontinuously. The family of experimental stress-relaxation curves will be represented by $\sigma_1(t, \varepsilon)$.

Second, the stress-strain curve for loading at constant strain rate should bear some relation to the loading phase of an impact. The family of these experimental curves will be represented by $\sigma_2(\varepsilon, \dot{\varepsilon})$, with the understanding that $\varepsilon = \dot{\varepsilon} t$ on each curve.

Third, the stress-strain curve for unloading at constant strain rate must bear some relation to the unloading phase of an impact. The shape of the unloading curve should depend on the maximum strain ε^* reached in the loading phase, but may be independent of the loading curve shape at high strain rates. Only that part of the unloading curve between the loaded and zero-stress states is of interest, and will be represented by $\sigma_3(\varepsilon, \dot{\varepsilon}, \varepsilon^*)$ with ε proportional to $\dot{\varepsilon} t$ on the curve. Also, continuity between stress states at the instant of load reversal requires that the expression for σ_3 reduce to the expression for σ_2 when $\varepsilon = \varepsilon^*$.

Fourth, any material model should possess consistent asymptotic characteristics, i.e., the stress responses to the relaxation and stress-strain tests should converge at long times and low strain rates, respectively, to the same asymptotic stress-strain curve $\sigma_\infty(\varepsilon)$. If $\sigma_1, \sigma_2, \sigma_3$, and σ_∞ are a set of candidate functions, each of which suitably represents its assigned behavior aspect, then the model consistency requirements are:

$$\sigma_1(t,\varepsilon) \to \sigma_\infty(\varepsilon) \text{ as } t \to \infty \tag{35a}$$

$$\sigma_2(\varepsilon,\dot{\varepsilon}) \text{ and } \sigma_3(\varepsilon,\dot{\varepsilon},\varepsilon^*) \to \sigma_\infty(\varepsilon) \text{ as } \dot{\varepsilon} \to 0 \tag{35b}$$

The conditions of consistency are satisfied by the family of constitutive equations:

$$\dot{\sigma} + \sigma/\tau = S(\varepsilon,\dot{\varepsilon}) \tag{36}$$

where $S(\varepsilon,\dot{\varepsilon})$ is any continuous function of strain and strain rate and where (for the moment) attention is focussed on the loading behavior. Proof of this proposition is straightforward. The asymptotic stress-strain behavior is obtained directly from Eq. 36 by recognizing that $\dot{\sigma} \to 0$ as $\dot{\varepsilon} \to 0$, i.e.:

$$\sigma_2 = \tau S(\varepsilon,0) = \sigma_\infty(\varepsilon) \tag{37}$$

For stress-relaxation behavior, the general solution of Eq. 36 is given by[2]:

$$\sigma_1(t,\varepsilon) = e^{-t/\tau}\left[A + \int S(\varepsilon,\dot{\varepsilon}) e^{t/\tau} dt\right] \tag{38}$$

For the conditions of stress relaxation, $\dot{\varepsilon}=0$ and ε constant, Eq. 38 reduces to:

$$\sigma_1(t,\varepsilon) = Ae^{-t/\tau} + \tau S(\varepsilon,0) \tag{39}$$

Hence, $\sigma_1(t,\varepsilon) \rightarrow \tau S(\varepsilon,0)$ as $t \rightarrow \infty$, which proves the proposition. The foregoing proof also holds for functions $S(\varepsilon,\dot{\varepsilon},\varepsilon^*)$ which satisfy stress-state continuity at reversal from loading to unloading.

The LVS model (Section 2.1) is a member of the family defined by Eq. 36. Other members can involve nonlinear functions of strain and strain rate, but the family has the property of a single characteristic decay time. It remains to be seen, therefore, whether another member can be found to suitably represent real material behavior. The stress-relaxation test results for Ensolite foam rubber appeared to suggest such a possibility (see Figure 2-3 in Volume I).

3.2 NINE-PARAMETER MODEL

An empirical model containing nine parameters was developed for application to Ensolite foam rubber as follows. First, candidate functions σ_2 and σ_3 were selected to represent the stress-strain test results. Second, the candidate functions were used to derive the forms of $S(\varepsilon,\dot{\varepsilon})$ and $S(\varepsilon,\dot{\varepsilon},\varepsilon^*)$ for the loading and unloading branches of the constitutive equation. Finally, the constitutive equation was used to derive the other behavior functions σ_1 and σ_∞.

The following function was selected to represent the loading phase of a stress-strain test:

$$\sigma_2(\varepsilon,\dot{\varepsilon}) = \frac{\varepsilon^m}{(1-\varepsilon)^n}(E_\infty + E_r\dot{\varepsilon}^r) \tag{40}$$

The exponents m, n, r respectively, provide a strain-softening characteristic, a strain-stiffening characteristic, and sensitivity of stress to strain rate. The two remaining parameters E_∞ and E_r are moduli. This function is thus equipped to represent the type of behavior evident in the loading branches of the stress-strain curves shown in Figure 2-8.

Some additional consideration was required before selecting a candidate function for unloading. Examination of Figure 2-8 led to the observations that, after unloading, the residual strain tended to increase rapidly with increasing strain rate, and that large residual strain correlated with difference between the shapes of the loading and unloading curves.

However, these observations are based on the results of tests in which the maximum strain ε^* is of the order of 0.8, while the material model must be able to deal with both smaller and larger values of ε^*. For smaller values of ε^*, it was assumed that the residual strain would be proportionately reduced, and that the shape of the unloading curve would more closely resemble the shape of the loading curve. To deal with larger values of ε^*, it was assumed that the residual strain would be proportionately increased up to a limiting value associated with the asymptotic case $\varepsilon^* \to 1$.

The following function was consequently selected to represent the unloading phase of a stress-strain test:

$$\sigma_3(\varepsilon, \dot{\varepsilon}, \varepsilon^*) = \frac{\varepsilon - \varepsilon^* (\tau^* \dot{\varepsilon})^p}{\varepsilon \left[1 - (\tau^* \dot{\varepsilon})^p\right]} \sigma_2(\varepsilon, \dot{\varepsilon}) \tag{41}$$

where it is to be understood that the magnitude of $\dot{\varepsilon}$ is to be used in this equation, since $\dot{\varepsilon} < 0$ for unloading. For $\varepsilon = \varepsilon^*$, Eq. 41 reduces to Eq. 40, i.e., Eq. 41 satisfies the requirement for stress continuity at load reversal. The term $(\tau^* \dot{\varepsilon})^p$ represents the limiting value of residual strain; the parameters τ^*, p provide a scale factor and a power-law behavior for the limiting residual strain as a function of strain rate.

The effect of Eq. 41 is to create a linear mapping of a part AB of the loading curve to produce the unloading curve shape. Figure 3-1 schematically illustrates the mapping effect.

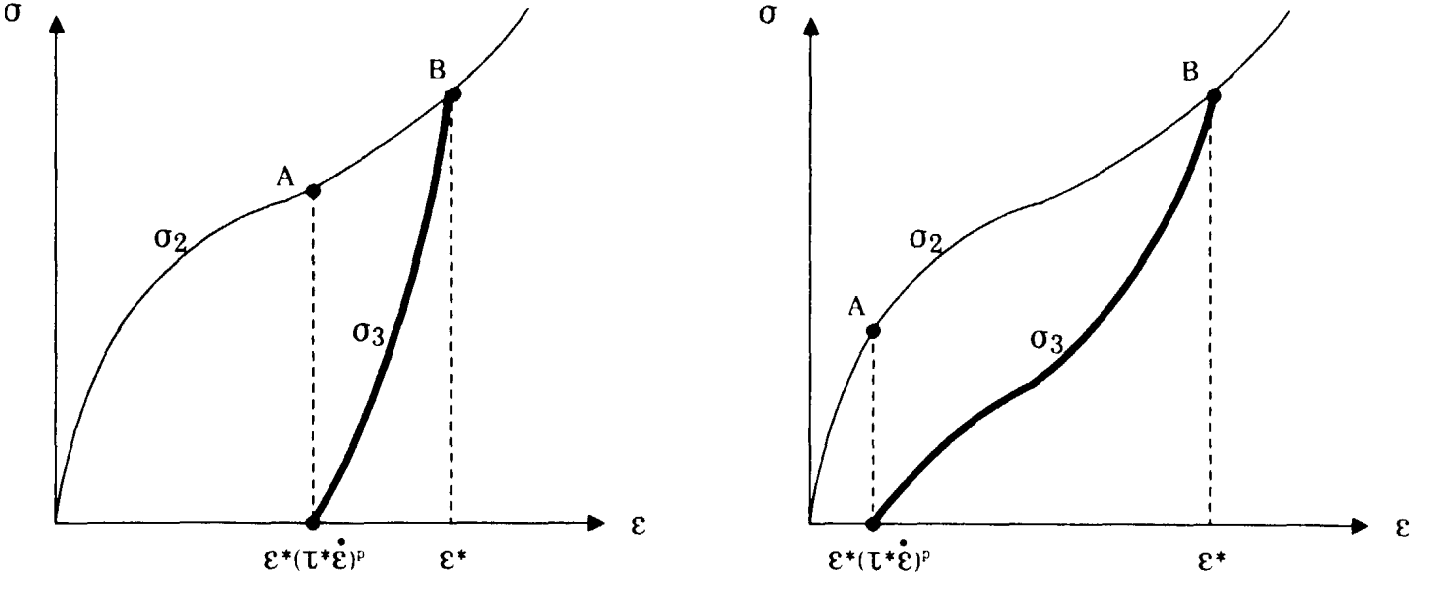

(A) AT HIGH STRAIN RATE

(B) AT LOW STRAIN RATE

FIGURE 3-1. MAPPING EFFECT OF UNLOADING FUNCTION

The function $S(\varepsilon, \dot{\varepsilon})$ for the loading branch of the constitutive equation can now be obtained by substituting σ_2 in the left hand side of Eq. 36, and by noting that $\dot{\sigma} = \dot{\varepsilon} \frac{d\sigma}{d\varepsilon}$ because $\varepsilon = \dot{\varepsilon} t$ on the stress-strain curve. This leads immediately to:

$$S(\varepsilon,\dot{\varepsilon}) = \dot{\varepsilon} d\sigma_2/d\varepsilon + \sigma_2/\tau$$

$$= \frac{\varepsilon^m}{(1-\varepsilon)^n}(E_\infty + E_r \dot{\varepsilon}^r)\left(\frac{m\dot{\varepsilon}}{\varepsilon} + \frac{n\dot{\varepsilon}}{1-\varepsilon} + \frac{1}{\tau}\right) \tag{42}$$

In a similar manner, the unloading branch is derived as:

$$S(\varepsilon,\dot{\varepsilon},\varepsilon^*) = \frac{\varepsilon^{m-2}\varepsilon^*(\tau^*\dot{\varepsilon})^p(E_\infty + E_r\dot{\varepsilon}^r)}{(1-\varepsilon)^n[1-(\tau^*\dot{\varepsilon})^p]} \tag{43}$$

$$+ \frac{\varepsilon - \varepsilon^*(\tau^*\dot{\varepsilon})^p}{\varepsilon[1-(\tau^*\dot{\varepsilon})^p]} S(\varepsilon,\dot{\varepsilon})$$

The remaining behavior functions can now be found by combining Eqs. 38 and 42, which leads immediately to the stress-relaxation equation:

$$\sigma_1(t,\varepsilon) = Ae^{-t/\tau} + \frac{E_\infty \varepsilon^m}{(1-\varepsilon)^n} = \frac{[E_\infty + (E_o - E_\infty)e^{-t/\tau}]\varepsilon^m}{(1-\varepsilon)^n} \tag{44}$$

Also apparent from Eq. 44 is the asymptotic stress-strain function:

$$\sigma_\infty(\varepsilon) = \frac{E_\infty \varepsilon^m}{(1-\varepsilon)^n} \tag{45}$$

The complete constitutive equation of the nine-parameter model:

$$\dot{\sigma} + \sigma/\tau = \begin{cases} S(\varepsilon,\dot{\varepsilon}) \text{ for } \dot{\varepsilon} \geq 0 \\ S(\varepsilon,|\dot{\varepsilon}|,\varepsilon^*) \text{ for } \dot{\varepsilon} < 0 \end{cases} \tag{46}$$

actually makes use of only eight parameters: the decay time τ; the moduli E_∞ and E_r; the scaling factor τ^*; and the exponents m,n,p,r. The ninth parameter, E_o, is not actually required unless one wishes to compute a response to the idealized stress-relaxation test described in Section 2.1(a).

3.3 MODEL WITH TWENTY-ONE PARAMETERS

As will be seen in Section 4, the ability of the nine-parameter model to fit the Ensolite foam rubber test data was questionable in some respects, particularly with regard to stress-relaxation behavior. Therefore, a second model was developed to provide additional time-scaling flexibility. The loading-to-unloading mapping properties of Eq. 43 and the stress-strain nonlinearity of Eq. 45 were retained in the second model. The added flexibility was achieved by means of a strain-dependent rate exponent in the loading stress-strain curve and a strain-dependent decay time in the stress-relaxation function. Accordingly, Eqs. 40 and 44 were replaced by the following functions:

$$\sigma_2(\varepsilon,\dot{\varepsilon}) = \sigma_\infty(\varepsilon) + \sigma_r\dot{\varepsilon}^r \exp(-\varepsilon^u/v)\left[\exp(\varepsilon^w/x) - \exp(\varepsilon^y/z)\right] \tag{47}$$

$$\sigma_1(t,\varepsilon) = \sigma_\infty(\varepsilon) + \sigma_o\exp(-t^A/BC^\varepsilon)\left[\exp(\varepsilon^a/b) - \exp(-\varepsilon^c/d)\right] \tag{48}$$

where $\sigma_\infty(\varepsilon)$ is given by Eq. 45, and where $\sigma_o,\sigma_r,A,B,C,a,b,c,d,r,u,v,w,x,y,z$ are new parameters. The parameters E_∞,m,n, τ^*, p are retained from the earlier model.

The new model contains 21 parameters, of which 16 appear in the constitutive equation. The constitutive equation, derived as outlined in Section 3.2, is as follows:

$$\dot{\sigma} + S(\varepsilon,\dot{\varepsilon}) - (At^{A-1}/BC^\varepsilon)\sigma \qquad (\dot{\varepsilon}\geq 0) \tag{49}$$

$$\dot{\sigma} = \frac{\dot{\varepsilon}\varepsilon^*(\tau^*|\dot{\varepsilon}|)^p}{\varepsilon^2[1-(\tau^*|\dot{\varepsilon}|)^p]}\left[\frac{E_\infty\varepsilon^m}{(1\ \ )^n} + \sigma_r|\dot{\varepsilon}|^r\exp(-\varepsilon^u/v)\left\{\exp(\varepsilon^w/x)-\exp(-\varepsilon^y/z)\right\}\right]$$
$$+ \frac{\varepsilon-\varepsilon^*(\tau^*|\dot{\varepsilon}|)^p}{\varepsilon[1-(\tau^*|\dot{\varepsilon}|^p]}\ S(\varepsilon,\dot{\varepsilon}) - (At^{A-1}/BC^\varepsilon)\sigma \qquad (\dot{\varepsilon}<0) \tag{50}$$

$$S(\varepsilon,\dot{\varepsilon}) = \frac{E_\infty \varepsilon^m}{(1-\varepsilon)^n}\left[\frac{m\dot{\varepsilon}}{\varepsilon} + \frac{n\dot{\varepsilon}}{1-\varepsilon} + \frac{At^{A-1}}{BC^\varepsilon}\right]$$

$$+ \sigma_r|\dot{\varepsilon}|^r \exp(-\varepsilon^u/v)\left[\frac{\dot{\varepsilon}}{\varepsilon}\left\{\frac{w}{x}\varepsilon^w \exp(\varepsilon^w/x) + \frac{y}{z}\varepsilon^y \exp(-\varepsilon^y/z)\right\}\right. \quad (51)$$

$$\left. + \left\{\frac{At^{A-1}}{BC^\varepsilon} - \frac{\dot{\varepsilon} ru}{\varepsilon v}\varepsilon^u \ln|\dot{\varepsilon}| \exp(-\varepsilon^u/v)\right\}\left\{\exp(\varepsilon^w/x) - \exp(-\varepsilon^y/z)\right\}\right]$$

3.4 CURVE-FITTING PROCEDURES

Least-squares regression formulas were developed to fit the model parameters to the laboratory test data. Linear regression formulas were derived by taking logarithms of the behavior-aspect equations. The resulting procedures were straightforward for the 9-parameter model but not for the 21-parameter model.

3.4.1 Regression Formulas for 9-Parameter Model

The basis of the approach to curve-fitting is to deal with groups of parameters, taking advantage of previous results at each step. In the first step, attention is focussed on the asymptotic parameters E_∞ ,m,n which appear in Eq. 45 for $\sigma_\infty(\varepsilon)$. In logarithmic form Eq. 45 becomes:

$$\log\sigma_\infty = \log E_\infty + m\log\varepsilon - n\log(1-\varepsilon) \quad (52)$$

Now assume that there are N asymptotic data points ($\varepsilon_i, \sigma_{\infty i}$) available. Then the square error associated with fitting Eq. 52 to these data points is given by:

$$(\Delta_\infty)^2 = \sum_{i=1}^{N}\left[\log E_\infty + m\log\varepsilon_i - n\log(1-\varepsilon_i) - \log\sigma_{\infty i}\right]^2 \quad (53)$$

and simultaneous linear equations in $\log E_\infty$,m,n can be derived by minimizing ($\Delta_\infty)^2$ w th respect to these parameters.

In the second step, attention is focussed on the parameters E_0 and σ which appear in Eq. 44 for the stress-relaxation behavior $\sigma_1(t, \varepsilon)$. Equation 44 can be rewritten as:

$$(1-\varepsilon)^n \varepsilon^{-m}\sigma_1 - E_\infty = (E_0 - E_\infty)e^{-t/\tau} \quad (54)$$

This leads to the square-error expression:

$$(\Delta_1)^2 = \sum_{i=1}^{N} \left[\log (E_o - E_\infty) - t_i/\tau - \log \left((1-\varepsilon_i)^n \varepsilon_i^{-m} \sigma_{1i} - E_\infty \right) \right]^2 \quad (55)$$

in terms of the stress-relaxation test data points $(\varepsilon_i, \sigma_{1i}, \tau_i)$. The values of E_∞ ,m,n are assumed to be as given by the first step, and $(\Delta_1)^2$ is minimized to derive simultaneous linear equations for $\log(E_o - E_\infty)$ and $1/\tau$.

In the third step, Eq. 40 for the loading stress-strain curve is rewritten in a manner similar to the procedure used in the second step, leading to the square error:

$$(\Delta_2)^2 = \sum_{i=1}^{N} \left[\log E_r + r \log \dot{\varepsilon}_i - \log \left((1-\varepsilon_i)^n \varepsilon_i^{-m} \sigma_{2i} - E_\infty \right) \right]^2 \quad (56)$$

in terms of the stress-strain test data points $(\varepsilon_i, \dot{\varepsilon}_i, \sigma_{2i})$. The values of E_∞ ,m,n are again assumed to be as given before, and $(\Delta_2)^2$ is minimized to derive equations for E_r and r.

The fourth and last step determines the values of the residual strain parameters τ^* and p. These parameters appear in Eq. 41 in the term:

$$\varepsilon_o = \varepsilon^* (\tau^* \dot{\varepsilon})^p \quad (57)$$

where ε_o is here defined as the residual strain after unloading from the maximum strain ε^* in a stress-strain test at the strain rate $\dot{\varepsilon}$. The square-error expression corresponding to Eq. 57 is:

$$(\Delta_3)^2 = \sum_{i=1}^{N} \left[(1/p) \log (\varepsilon_{oi}/\varepsilon_i^*) - \log \tau^* - \log \dot{\varepsilon}_i \right]^2 \quad (58)$$

in terms of the stress-strain test data points $(\dot{\varepsilon}_i, \varepsilon^*, \varepsilon_{oi})$, and minimization leads to simultaneous equations in 1/p and $\log \tau^*$.

3.4.2 Regression Formulas

The first and fourth steps in curve-fitting the 21-parameter model are identical to the corresponding steps for the 9-parameter model. The second and third steps require some additional consideration, however, because of the complexity of the modified behavior functions introduced in Eqs. 47 and 48.

The loading stress-strain function in Eq. 47 can be rewritten in the form:

$$\sigma_2 - E_\infty \varepsilon^m / (1-\varepsilon)^n = \sigma^*(\varepsilon) |\dot{\varepsilon}|^{r^*(\varepsilon)} \tag{59}$$

where

$$\sigma^*(\varepsilon) = \sigma_r \left[\exp(\varepsilon^w / x) - \exp(-\varepsilon^y / z) \right] \tag{60}$$

The functions σ^* and r^* are first treated as intermediate parameters by grouping stress-strain test data points into subsets ($\dot{\varepsilon}_i, \sigma_{2i}$) for individual values of strain. The values of σ^* and r^* can then be determined by regression of:

$$r^*(\varepsilon) = r \exp(-\varepsilon^u / v) \tag{61}$$

$$\Delta^2 = \sum_{i=1}^{N} \left\{ \log\sigma^* - r^* \log\dot{\varepsilon}_i - \log\left[\sigma_{2i} - E_\infty \varepsilon_i^m / (1-\varepsilon_i)^n \right] \right\}^2 \tag{62}$$

from Eq. 59. The remaining steps involve estimation of the model parameters in two subgroups by using σ^* and r^* in Eqs. 60 and 61, respectively.

A heuristic approach has been taken with respect to Eq. 60. The form of the strain function in brackets is such that its value is zero at $\varepsilon = 0$ and large when ε is large. Hence, one can choose an intermediate strain for which the function should have a unit value, and one can then choose σ_r to be the value of σ^* at the intermediate strain (in the case of the Ensolite test data, an intermediate strain between 0.15 and 0.2 appeared to be a good choice). The form of the strain function also leads one to expect that $\exp(\varepsilon^w/x) \to 1$ much faster than $\exp(-\varepsilon^y/z) \to 1$ as $\varepsilon \to 0$, ie., $\exp(\varepsilon^w/x) \cong 1$ for small strains. Conversely $\exp(-\varepsilon^y/z) \to 0$ rapidly for large strains.

The heuristic estimation procedure is then as follows. With $\sigma_r = \sigma^*(\varepsilon_{int})$ at the intermediate strain, Eq. 60 is replaced by the two estimation formulas:

$$\sigma^*(\varepsilon) = \sigma_r[\,1 - \exp(-\varepsilon^y/z)\,] \quad \text{for } \varepsilon < \varepsilon_{INT} \tag{63}$$

$$\sigma^*(\varepsilon) + \sigma_r \exp(-\varepsilon^y/z) = \sigma_r \exp(\varepsilon^w/x) \quad \text{for } \varepsilon > \varepsilon_{INT} \tag{64}$$

The square-error expression corresponding to Eq. 63 is:

$$\Delta^2 = \sum_{i=1}^{N} \left\{ y\log\varepsilon_i - \log z - \log\log\left[\frac{\sigma_r}{\sigma_r - \sigma^*(\varepsilon_i)}\right]\right\}^2 \tag{65}$$

for the parameters y, logz in terms of small-strain data. Corresponding to Eq. 64:

$$\Delta^2 = \sum_{i=1}^{N} \left\{ w\log\varepsilon_i - \log x - \log\log\left[\frac{\sigma^*(\varepsilon_i) + \sigma_r \exp(-\varepsilon_i^y/z)}{\sigma_r}\right]\right\}^2 \tag{66}$$

for the parameters w,logx in terms of large-strain data. The term $\exp(-\varepsilon_i y/z)$ in Eq. 66 is based on the previously calculated values for y and z, and has been included to improve the accuracy of the procedure when the large-strain data points include strains not much larger than ε_{int}.

The foregoing set of procedures involves approximations. Therefore, it is also necessary to iterate the estimates for w,x,y,z obtained from Eqs. 65 and 66.

The remaining parameters are estimated from Eq. 61. The form of the strain function in this equation is such that $r = r^*(0)$, and a heuristic approach is again required. In this case, the procedure is to choose $r = r^*(\varepsilon)$ for the smallest value of strain available in the data base. The last two parameters u,logv can then be calculated from the square error:

$$\Delta^2 = \sum_{i=1}^{N} \left\{ u\log\varepsilon_i - \log v - \log\log\left[\frac{r}{r^*(\varepsilon_i)}\right]\right\}^2 \tag{67}$$

The stress-relaxation function in Eq. 48 is treated in a similar manner by rewriting in the form:

$$\sigma_1 - E_\infty \varepsilon^m/(1-\varepsilon)^n = \sigma^*(\varepsilon)\exp(-t^A/BC^\varepsilon) \tag{68}$$

where

$$\sigma^*(\varepsilon) = \sigma_o\left[\exp(\varepsilon^a/b) - \exp(-\varepsilon^c/d)\right] \tag{69}$$

From Eq. 68, one recognizes that $\sigma^*(\varepsilon)$ is an "instantaneous stress" function. The stress-relaxation test data does not include points at times sufficiently short to approximate $\sigma^*(\varepsilon)$, however, as was discussed in Section 2.1 of Volume I. Therefore, stress-strain test data from tests at extremes of high strain rate and low temperature was used to estimate $\sigma^*(\varepsilon)$ in the present case.

The first sub-group of parameters is then iteratively estimated by a heuristic procedure analogous to Eqs. 63 through 66, i.e. $\sigma_o = \sigma^*(\varepsilon_{int})$ and

$$\Delta^2 = \sum_{i=1}^{N}\left\{c\log\varepsilon_i - \log d - \log\log\left[\frac{\sigma_o}{\sigma - \sigma^*(\varepsilon_i)}\right]\right\}^2 \quad \text{for } \varepsilon_i < \varepsilon_{int} \tag{70}$$

$$\Delta^2 = \sum_{i=1}^{N}\left\{a\log\varepsilon_i - \log b - \log\log\left[\frac{\sigma^*(\varepsilon_i) + \sigma_o \exp(-\varepsilon_i^c/d)}{\sigma_o}\right]\right\}^2 \quad \text{for } \varepsilon_i > \varepsilon_{int} \tag{71}$$

where, in the present case, $\varepsilon_{int} = 0.5$ was found to be a good choice for the Ensolite test data. The final three parameters A, logB, logC can then be estimated from the square error:

$$\Delta^2 = \sum_{i=1}^{N}\left\{A\log t_i - \log B - \varepsilon_i \log C - \log\log\left[\frac{\sigma_o[\exp(\varepsilon_i^a/b) - \exp(-\varepsilon_i^c/d)}{\sigma_{1i} - E_\infty \varepsilon_i^m/(1-\varepsilon_i)^n}\right]\right\} \tag{72}$$

in terms of stress-relaxation data points ($\varepsilon_i, \sigma_{1i}, t_i$).

4. APPLICATION OF MODELS TO TEST DATA

The 9- and 21- parameter empirical models were applied to the test data developed for Ensolite AAC foam rubber and reported in Volume I, using the curve-fitting procedures described in Section 3.4. Some smoothing of the test data was done before the models were curve-fitted.

4.1 DATA SMOOTHING AND INPUT

Data points from stress-strain tests at low strain rate (0.0012 per second) were used as input for fitting the asymptotic parameters E_∞ ,m,n. Smoothed stress-relaxation data was generated from the test results by reading data points from the time-temperature-superposition master curves (see Volume I, Figure 2-3).

The stress-strain master curves (see Volume I, Figure 3-3) were avoided, however, because they fell below the high-rate test data. Instead, the high-rate test data points were averaged at each value of strain rate to provide input for the loading stress-strain behavior.

High-rate data should also have been used to calculate the residual strain parameters, but measurements of the residual strain were found to be inaccurate at strain rates exceeding 73 per second. Lower strain-rate data was used, therefore, and consequently this part of the model can only be considered as an extrapolation for impact strain rates.

4.2 RESULTS FOR MODEL PARAMETERS

Tables 4-1 and 4-2 summarize the parameter values for the 9- and 21-parameter models, respectively. The parameters E_∞ ,m,n, τ^*,p are the same for the two models. The parameters τ and τ^* are reported in units of milliseconds (ms). Each table gives reference to the corresponding behavior-function equations and to comparison plots discussed in the next section.

TABLE 4-1. RESULTS FOR 9-PARAMETER MODEL

PARAMETER	VALUE	STANDARD ERROR	EQ.	FIG.
E_∞ (psi)	7.69	0.86 psi	45	10
m	0.675			
n	1.09			
E_0 (psi)	22.12	10.80 psi	44	12
τ (ms)	8.81			
E_r (psi)	5.45	5.90 psi	42	13
r	0.1666			
τ^* (ms)	0.00976	0.00948	57	11
p	0.0987			

TABLE 4-2. RESULTS FOR 21-PARAMETER MODEL

PARAMETER	VALUE		STANDARD ERROR	EQ.	FIG.
E_∞	7.69	psi	0.86 psi	45	10
m	0.675				
n	1.09				
$\sigma 0$	66.0	psi	0.96	48	12
A	0.130				
B	0.156				
C	3.08				
a	10.12				
b	0.279				
c	1.94				
d	0.0290				
σr	4.153	psi	1.25 psi	47	13
r	0.190				
u	3.17				
v	0.580				
w	2.57				
x	0.296				
y	2.23				
z	0.00164				
τ^* (ms)	0.00976	sec	0.00948	57	11
p	0.0987				

The tables also report standard errors for each group of parameters. The standard error measures the inaccuracy of the curve fit with respect to the input data points. For example:

$$\text{Standard Error} = \sqrt{\frac{1}{N}\sum_{i=1}^{N}\left(\sigma_\infty(\varepsilon_i) - \sigma_{\infty i}\right)^2} \tag{73}$$

measures the deviation of $\sigma_\infty(\varepsilon_i)$, as calculated by Eq. 45, from the input data points $\sigma_{\infty i}$. The second and third groups have standard errors related to the stress-relaxation function σ_1 and the stress-strain function σ_2, respectively. The standard error of the fourth group is related to the residual strain function ε_o (Eq. 57).

Note that the errors in σ_1 and σ_2 are comparable to the values of the respective modulus parameters for the 9-parameter model. This is an indication of poor fit. Conversely, these errors are much smaller in relation to the modulus parameters of the 21-parameter model.

4.3 COMPARISON OF BEHAVIOR CURVES WITH INPUT DATA

Figures 4-1 through 4-4 compare the empirical model behavior curves with the input data from which the model parameters were calculated. Figures 4-1 and 4-2 compare the asymptotic and residual strain behavior, respectively. These plots apply to both models, and they show that the models fit these behavior aspects well.

Figures 4-3 and 4-4 illustrate the stress-relaxation and stress-strain behaviors, respectively. The improvement in fit provided by the 21-parameter model over the 9-parameter model is evident in both cases.

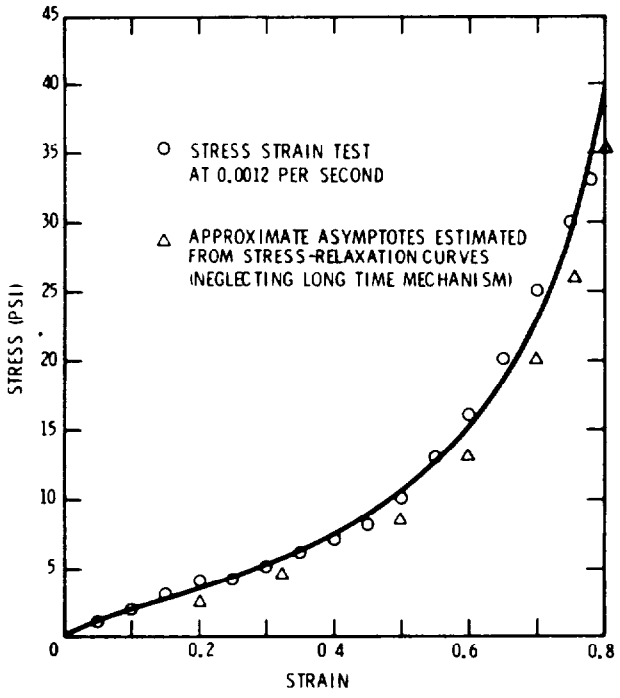

FIGURE 4-1. ASYMPTOTIC BEHAVIOR

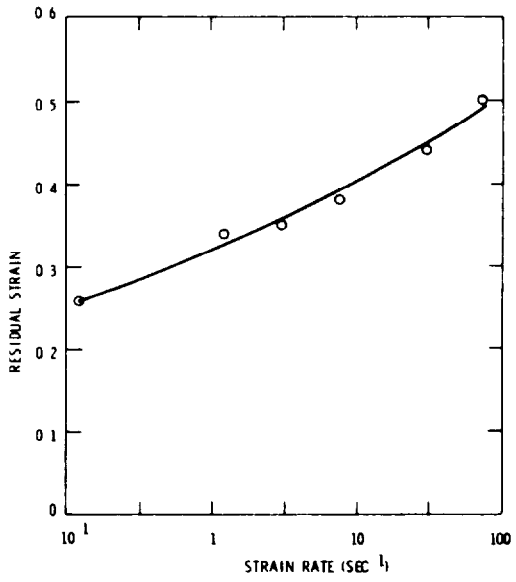

FIGURE 4-2. RESIDUAL STRAIN BEHAVIOR

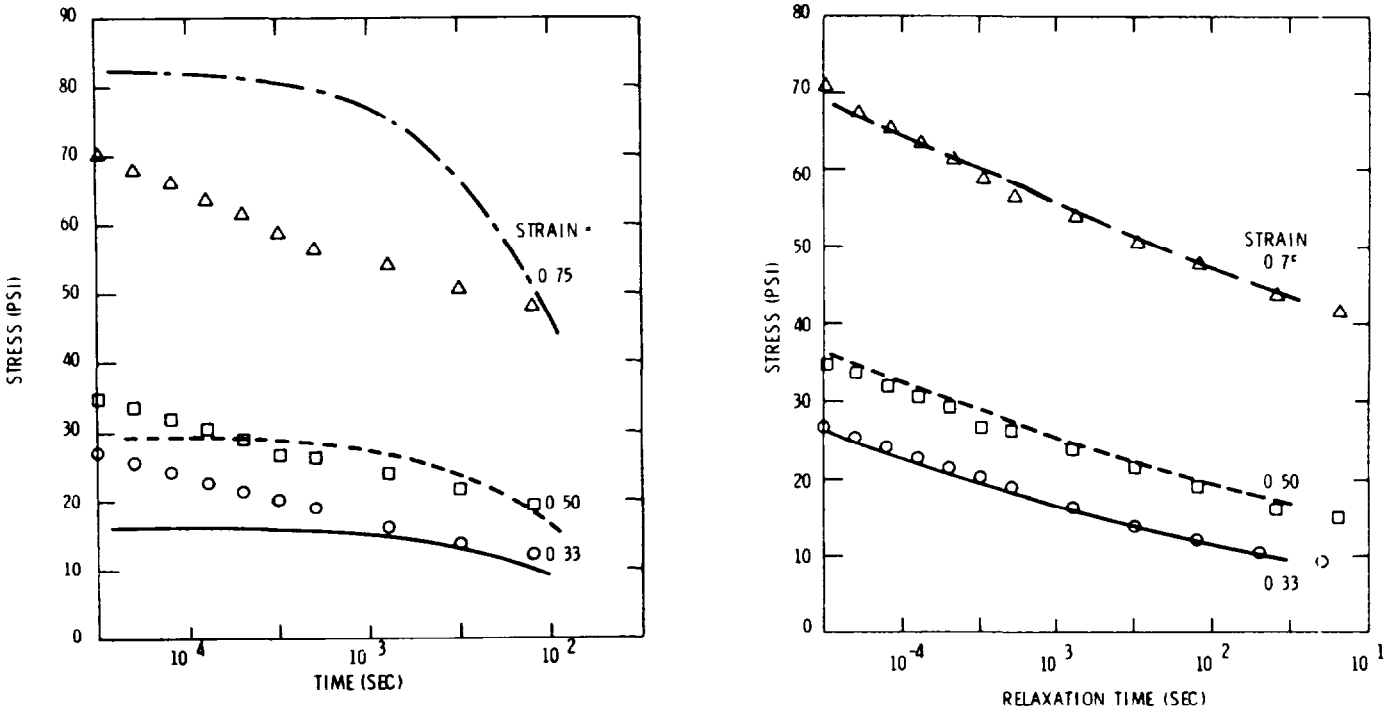

(A) 9-Parameter Model

(B) 21-Parameter Model

FIGURE 4-3. STRESS-RELAXATION BEHAVIOR

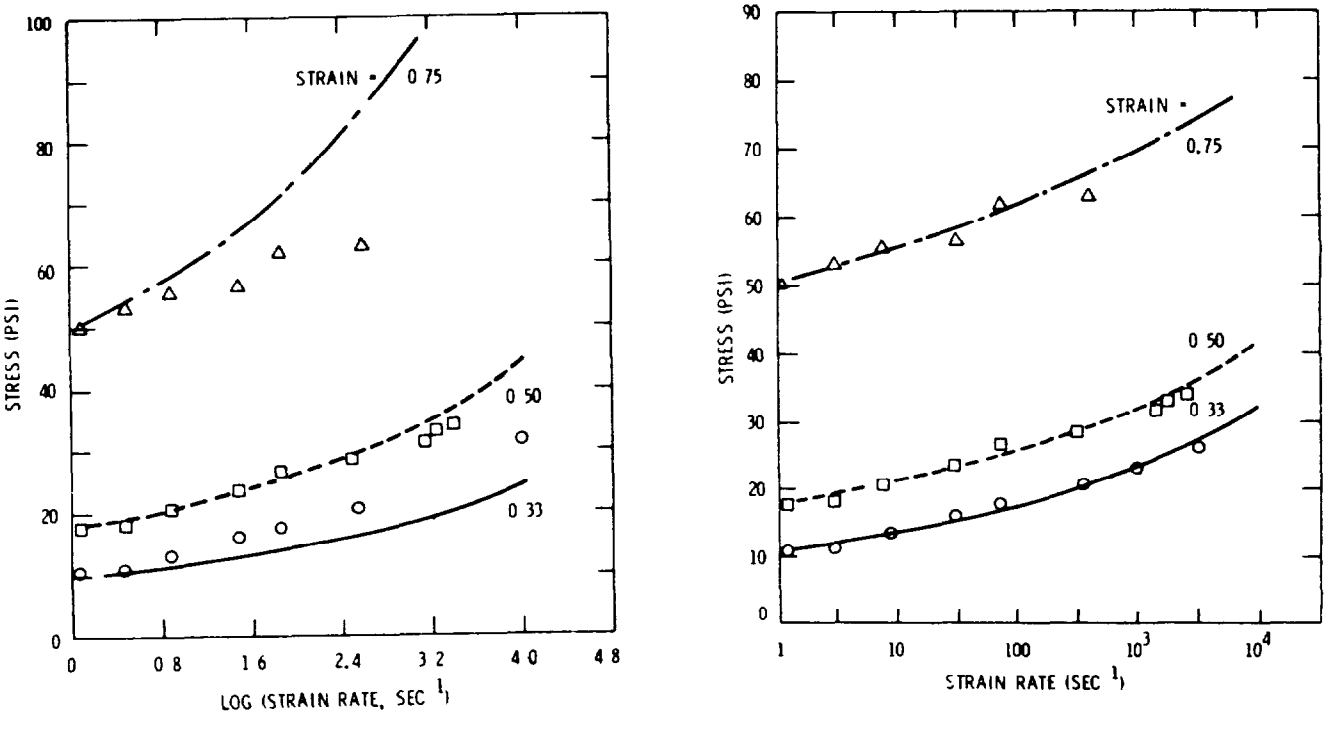

(A) 9-Parameter Model

(B) 21-Parameter Model

FIGURE 4-4. STRESS-STRAIN BEHAVIOR

5. CONCLUSIONS

The research reported herein comprises an investigation and development of one-dimensional constitutive equation models for application to crash padding materials and the application of two models to laboratory test data previously developed for Uniroyal Ensolite AAC foam rubber. The following conclusions can be drawn from the results of the research:

- Neither conventional material models such as the linear viscoelastic solid nor empirical models with only a few parameters based on limited aspects of observed behavior are sufficiently flexible to accurately describe the dynamic behavior of real viscoelastic materials with strong nonlinearities.

- Nonlinear viscoelastic material behavior can be described by multi-parameter empirical models. Such models can be formulated in accordance with conditions of mathematical consistency, an approach which leads to a useful constitutive equation. The constitutive equation is the essential basis for prediction of material response under dynamic conditions other than standard laboratory tests.

- Least-squares estimation procedures can be developed for multi-parameter models in a way such that the parameters can be fitted to materials test data in an organized approach. This approach takes advantage of the entire test data base, i.e., the parameter estimates are unbiased.

- The two models that were developed and applied to the Ensolite test data contain 9 and 21 parameters, respectively. The 9-parameter model is easy to fit and work with but represents the material poorly at short times and high strain rates. The 21-parameter model is difficult to fit and work with but represents the material well over the entire dynamic range of interest.

- Both the 9- and 21- parameter models can be applied in principle to test data gathered on other viscoelastic materials which might be candidates for crash padding.

APPENDIX
HP67 PROGRAMS FOR NONLINEAR-SPRING MODELS OF CONSTITUTIVE EQUATIONS

This appendix contains two programs based on Eqs. 28 and 30. The first simulates the idealized stress-relaxation test and is discussed in Section A.1. The second simulates the stress-strain test at constant strain rate (see Section A.2). Both programs have options for either softening or stiffening behavior.

The finite-difference algorithm for the softening model is given by:

$$\sigma_{k+1} = \sigma_k + \left\{ \frac{\tau E_o \dot{\varepsilon}_k + E_\infty \varepsilon_k - [1+(E_\infty/B)(\sigma_k/B)^{n-1}]\ \sigma_k}{1+n\ (E_o/B)\ (\sigma_k/B)^{n-1}} \right\} h \qquad \text{(A.1)}$$

where $h = \Delta t/\tau$. The stiffening algorithm is given by:

$$\sigma_{k+1} = \sigma_k + \left\{ [1+n(B/E_o)\varepsilon_k^{n-1}]\ \tau E_o \dot{\varepsilon}_k + [1+(B/E_\infty)\varepsilon_k^{n-1}]\ E_\infty \varepsilon_k - \sigma_k \right\} h \qquad \text{(A.2)}$$

for stress relaxation $\dot{\varepsilon} = 0$ and ε is a constant. For the stress-strain test $\dot{\varepsilon}$ is a constant and $\varepsilon_k = kh\dot{\varepsilon}$.

A.1 Stress-Relaxation Program

The program starts from specified initial conditions ε *, σ *. For the softening model σ * is specified and the corresponding value of ε * is momentarily displayed before the time integration begins. For the hardening model ε* is specified and σ * is momentarily displayed before the time integration begins.

During the time integration, the program momentarily displays the current step number, H, and the current stress, σ_H, where H is a specified multiple of the nondimensional time step size h. At each step, the program tests the termination condition:

$$\left| (\sigma_{k+1} - \sigma_k)/\sigma_{k+1} \right| < 10^{-3} \qquad \text{(A.3)}$$

If this condition is satisfied, the program momentarily displays the last step number, k+1, the corresponding stress, σ_{k+1}, and then stops with a comparison value in the display. For the softening model, the comparison value is a strain ε^{**}, and the difference $\varepsilon^{*} - \varepsilon^{**}$ is an indirect measure of the degree to which the stress has relaxed. For the stiffening model, the comparison value is the asymptotic stress σ_∞, and $\sigma_{k+1} - \sigma_\infty$ measures the degree of relaxation.

The nature of the termination condition is such that the process of relaxation may be "stopped short" when a small time step size is chosen. If the error measure indicates that this has happened, then increase h by a factor of 10 and make a second run. (In general, the values h = 0.1 and h = 1.0 will cover the most significant range in the relaxation process.) If the termination condition leaves an unacceptably wide data gap between the two h-values, decrease the tolerance to 10^{-4} at program steps 057-060 and 126-129.

The following two pages document the program. Table A.1 gives a test example.

A.2 Stress-Strain Program

The program starts from $\varepsilon = \sigma = 0$ and simulates loading at a constant strain rate $\dot{\varepsilon}$ (specified by the nondimensional rate $\tau\dot{\varepsilon}$) up to a specified maximum strain ε^{*} in a specified number of increments M. When the maximum strain has been reached, the program immediately simulates unloading at the constant strain rate $-\dot{\varepsilon}$ from ε^{*} to zero strain. The time step size $h = \varepsilon^{*}/M\tau\dot{\varepsilon}$ is internally computed.

During execution, the program momentarily displays the step number H, the current strain ε_H, and the current stress σ_H, where H is a specified multiple of h. The step number is incremented during loading and decremented during unloading.

The program is supplied in a version which simulates softening behavior. To change to the stiffening model or back to the softening model, simply edit program steps 025 and 054 in accordance with:

SOFTENING: | g | GSBf | a |

STIFFENING: | g | GSBf | b |

Table A 2 gives a test example. The program listing appears on the two pages following Table A 2.

TABLE A-1. TEST EXAMPLE FOR STRESS-RELAXATION PROGRAM

USER STORES:			
	4 . 8	STO 1	B
	2 0	STO 2	E_o
	1 0	STO 3	E
	1 . 8	STO 4	n
	. 1	STO 6	h
	1 0	STO 7	H

SOFTENING		STIFFENING	
USER:	. 4 A	USER:	. 0 2 B
PROGRAM:		PROGRAM:	
	0.0314		0.4042
10	0.3263	10	0.2739
20	0.2907	20	0.2285
30	0.2744	30	0.2127
40	0.2670	40	0.2072
48	0.2642	45	0.2059
	0.0318		0.2042

TABLE A-2. TEST EXAMPLE FOR STRESS-STRAIN PROGRAM

USER STORES:

4 . 8 STO A	B
2 0 STO B	E_o
1 0 STO C	E_∞
1 . 8 STO D	n
1 0 STO 6	H
5 0 STO 7	M

SOFTENING

EDIT TO: g GSBf a

USER: . 5 ENTER ϵ^*
. 2 A $\tau\dot{\epsilon}$

PROGRAM:

```
10  0.1  0.9352
20  0.2  1.4437
30  0.3  1.8502
40  0.4  2.2031
50  0.5  2.5220
40  0.4  2.0890
30  0.3  1.6269
20  0.2  1.1056
10  0.1  0.4410
 0  0.0 -0.5668
```

STIFFENING

EDIT TO: g GSBf b

USER: . 5 ENTER ϵ^*
1 A $\tau\dot{\epsilon}$

PROGRAM:

```
10  0.1  1.9958
20  0.2  3.9695
30  0.3  5.9237
40  0.4  7.8647
50  0.5  9.7993
40  0.4  7.7394
30  0.3  5.6988
20  0.2  3.6754
10  0.1  1.6778
 0  0.0 -0.2969
```

HP-67 PROGRAM: STRESS RELAXATION (NONLINEAR-SARING MODELS)

REGISTER USAGE:

R0	R1	R2	R3	R4	R5	R6	R7	R8	R9	RA	RB	RC	RD	RE	
σ_k	B	E_0	E_∞	η	$E_\infty\epsilon^*$	h	H	(a)	(a)	(b)	(b)				SOFTENING
σ_k	B	E_0	E_∞	η	ϵ^*	h	H	(a)	(a)	(b)	σ_∞				STIFFENING

(a) - LOOP INDICES (b) - WORKING STORAGE

001	f	LBL	A	soft	029	RCL	4			057	•				085	RCL	A		
002	STO	0			030	h	y^x			058	0				086	+			ϵ^{**}
003	RCL	1			031	STO	B			059	0				087	h	RTN		
004	÷				032	RCL	2			060	1				088	f	LBL	B	stiff
005	RCL	4			033	X				061	g	x≷y			089	STO	5		
006	h	y^x			034	RCL	0			062	GTO	3			090	RCL	4		
007	STO	A			035	÷				063	RCL	8		k (mod II)	091	h	y^x		
008	RCL	0			036	RCL	4			064	RCL	7		H	092	RCL	1		
009	RCL	2			037	X				065	g	x≷y			093	X			
010	÷				038	1				066	GTO	2			094	STO	A		
011	RCL	A			039	+				067	RCL	9			095	RCL	5		
012	+			ϵ^*	040	STO	A		DENOM	068	h	PAUSE			096	RCL	2		
013	h	PAUSE			041	RCL	B			069	RCL	0			097	X			
014	RCL	3			042	RCL	3			070	h	PAUSE			098	RCL	A		
015	X				043	X				071	GTO	1			099	+			
016	STO	5			044	CHS				072	f	LBL	3		100	STO	0		σ^*
017	0				045	RCL	0			073	RCL	9			101	h	PAUSE		
018	STO	9			046	−				074	h	PAUSE			102	RCL	5		
019	f	LBL	1	DISP. LOOP	047	RCL	5			075	RCL	0			103	RCL	3		
020	0				048	+				076	h	PAUSE			104	X			
021	STO	8			049	RCL	6			077	RCL	1			105	RCL	A		
022	f	LBL	2	SLOOP	050	X			NUM	078	÷				106	+			
023	1				051	RCL	A			079	RCL	4			107	STO	B		σ_∞
024	STO	+	8		052	÷			$\Delta\sigma_k$	080	h	y^x			108	0			
025	STO	+	9		053	STO	+	0		081	STO	A			109	STO	9		
026	RCL	0			054	RCL	0			082	RCL	0			110	f	LBL	4	DISP LOOP
027	RCL	1			055	÷				083	RCL	3			111	0			
028	÷				056	h	ABS		$\lvert\Delta\sigma_k/\sigma_k\rvert$	084	÷				112	STO	8		

113	f	LBL	5	∫LOOP	141	f	LBL	6		169					197					
114	1				142	RCL	9			170					198					
115	STO	+	B		143	h	PAUSE			171					199					
116	STO	+	9		144	RCL	0			172					200					
117	RCL	B			145	h	PAUSE			173					201					
118	RCL	0			146	RCL	B			174					202					
119	−				147	h	RTN			175					203					
120	RCL	6			148					176					204					
121	×			.	149					177					205					
122	STO	+	0		150					178					206					
123	RCL	0			151					179					207					
124	÷				152					180					208					
125	h	ABS		$\lvert\frac{\sigma}{\sigma_x}\rvert$	153					181					209					
126	•				154					182					210					
127	0				155					183					211					
128	0				156					184					212					
129	1				157					185					213					
130	g	x>y			158					186					214					
131	GTO	6			159					187					215					
132	RCL	8		k (mod H)	160					188					216					
133	RCL	7		H	161					189					217					
134	g	x>y			162					190					218					
135	GTO	5			163					191					219					
136	RCL	9			164					192					220					
137	h	PAUSE			165					193					221					
138	RCL	0			166					194					222					
139	h	PAUSE			167					195					223					
140	GTO	4			168					196					224					

USER ACTIONS:

[B-value] [STO] [1] [E_o-value] [STO] [2] [E_∞-value] [STO] [3]

[n-value] [STO] [4] [h-value] [STO] [6] [H-value] [STO] [7]

Softening model:

[σ^*-value] [A]

Stiffening model

[ϵ^*-value] [B]

HP-67 PROGRAM: STRESS-STRAIN AT CONSTANT STRAIN RATE (NONLINEAR-SPRING MODELS)

REGISTER USAGE:

R0	R1	R2	R3	R4	R5	R6	R7	R8	R9	RA	RB	RC	RD	RE
σ_k	ϵ_k	ϵ^*	$\tau\dot{\epsilon}$	$E_0\tau\dot{\epsilon}$	h	H	M	k (mod H)	k	B	E_0	E_∞	n	WORK. STOR.

NOTE: INDEX REG RI ALSO USED AS WORKING STORAGE

001	f	LBL	A		029	STO	+	1		057	X			Δε	085	X			
002	STO	3			030	RCL	8		k (mod H)	058	STO	−	1		086	RCL	B		
003	h	↓			031	RCL	6		H	059	RCL	8		k (mod H)	087	X			
004	STO	2			032	g	x>y			060	RCL	6		H	088	RCL	A		
005	RCL	3			033	GTO	2			061	g	x>y			089	÷			
006	÷				034	RCL	9			062	STO	4			090	1			
007	RCL	7			035	h	PAUSE			063	RCL	9			091	+			DENOM
008	÷			h	036	RCL	1			064	h	PAUSE			092	STO	E		
009	STO	5			037	h	PAUSE			065	RCL	1			093	h	RCL		
010	RCL	B			038	RCL	0			066	h	PAUSE			094	RCL	0		
011	RCL	3			039	h	PAUSE			067	RCL	0			095	X			
012	X			$E_0\tau\dot{\epsilon}$	040	RCL	9		k	068	h	PAUSE			096	RCL	C		
013	STO	4			041	RCL	7		M	069	RCL	9		k	097	X			
014	0				042	g	x>y			070	f	x>0			098	RCL	A		
015	STO	0			043	GTO	1			071	GTO	3			099	÷			
016	STO	1			044	RCL	4			072	h	RTN			100	CHS			
017	STO	9			045	CHS				073	g	LBL	a	SOFT	101	RCL	D		
018	f	LBL	1	DISP. LOOP	046	STO	4		$-\tau\dot{\epsilon}$	074	RCL	D			102	−			
019	0				047	f	LBL	3	DISP LOOP	075	1				103	RCL	4		
020	STO	8			048	0				076	−				104	+			
021	f	LBL	2	∫LOOP	049	STO	8			077	RCL	0			105	RCL	C		
022	1				050	f	LBL	4	∫LOOP	078	RCL	A			106	RCL	1		
023	STO	+	8		051	1				079	÷				107	X			
024	STO	+	9	LOAD	052	STO	+	8		080	h	ABS			108	+			NUM
025	g	GSB	a	σ_{k+1}	053	STO	−	9	UNLOAD	081	h	$x \rightleftarrows y$			109	RCL	E		
026	RCL	5			054	g	GSB	a	σ_{k+1}	082	h	y^x			110	÷			
027	RCL	3			055	RCL	5			083	h	STI			111	RCL	5		
028	X			Δε	056	RCL	3			084	RCL	D			112	X			$\Delta\sigma_k$

113	STO	+	0		141					169					197					
114	h	RTN			142					170					198					
115	g	LBL$_c$	b	STIFF	143					171					199					
116	RCL	D			144					172					200					
117	1				145					173					201					
118	−				146					174					202					
119	RCL	1			147					175					203					
120	h	$x\hat{}y$			148					176					204					
121	h	y^x		.	149					177					205					
122	RCL	3			150					178					206					
123	RCL	1			151					179					207					
124	+				152					180					208					
125	×				153					181					209					
126	RCL	A			154					182					210					
127	×				155					183					211					
128	RCL	C			156					184					212					
129	RCL	1			157					185					213					
130	×				158					186					214					
131	+				159					187					215					
132	RCL	4			160					188					216					
133	+				161					189					217					
134	RCL	0			162					190					218					
135	−				163					191					219					
136	RCL	5			164					192					220					
137	×			$\Delta\sigma_k$	165					193					221					
138	STO	+	0		166					194					222					
139	h	RTN			167					195					223					
140					168					196					224					

USER ACTIONS:

[B-value] [STO] [A] [E_o-value] [STO] [B] [E_∞-value] [STO] [C]

[n-value] [STO] [D] [H-value] [STO] [6] [M-value] [STO] [7]

Softening (default program):

[ϵ^*-value] [ENTER] [$\tau\dot{\epsilon}$-value] [A]

Stiffening ([g] [GSB$_c$] [b] at steps 025 and 054):

[ϵ^*-value] [ENTER] [$\tau\dot{\epsilon}$-value] [A]

REFERENCES

1) W. Flugge, Viscoelasticity, Blaisdell Publishing Company, Waltham, MA 1967

2) G. B. Thomas, Jr., Calculus and Analytic Geometry, Part 2, Addison-Wesley Publishing Company, Reading, MA, 3rd edition, 1961.

3) A. V. Tobolsky, Properties and Structure of Polymers, Wiley, New York, 1967.

4) E. A. Meinecke and R. C. Clark, "Mechanical Properties of Polymeric Foams," Technomic Publishing Co., Westport, CT, 1973.

5) F. J. Lockett, R. R. Cousins, and D. Dawson, "Engineering Basis for Selection and Crash Padding Materials," Plastics and Rubber Processing and Applications, Vol. 1 No. 1 (1981), 25-37.

US Department
of Transportation

**Research and
Special Programs
Administration**

Kendall Square
Cambridge Massachusetts 02142

Official Business
Penalty for Private Use $300

Postage and Fees Paid
Research and Special
Programs Administration
DOT 513